REVISION 1

Experimental and Modeled Chlorine Solubilities in Aluminosilicate Melts at 1 to 7000 Bars and 700 to 1250°C: Applications to Magmas of Augustine Volcano, Alaska

JAMES D. WEBSTER[1], FRANCESCO VETERE[2], ROMAN E. BOTCHARNIKOV[2], BETH GOLDOFF[1], ALEXANDER MCBIRNEY[3], ANGELA L. DOHERTY[4]

[1]Department of Earth and Planetary Sciences, American Museum of Natural History, Central Park West at 79th Street, New York, NY, 10024-5192, U.S.A. E-mail: jdw@amnh.org
[2]Institut für Mineralogie, Leibniz Universtät Hannover, Callinstrasse 3, D-30167, Hannover, Germany
[3]Department of Geological Sciences, 1272 University of Oregon, Eugene, Oregon, 97403-1272, U.S.A.
[4]Dipartimento di Scienze della Terra, dell'Ambiente e delle Risorse, Università degli Studi di Napoli Federico II, Via Mezzocannone 8 – 80134 Naples, Italy

Submitted to the American Mineralogist
April 18, 2014
Revised version submitted
August 8, 2014

This is a preprint, the final version is subject to change, of the American Mineralogist (MSA)
Cite as Authors (Year) Title. American Mineralogist, in press.
(DOI will not work until issue is live.) DOI: http://dx.doi.org/10.2138/am-2015-5014

ABSTRACT

Hydrothermal experiments were conducted at ca. 1 to 7000 bars and 700 to 1250°C in 121 rhyolitic to basaltic systems to determine Cl solubility in silicate melts, i.e., the maximum Cl concentration in melts that are saturated in a hydrosaline liquid with or without an aqueous or aqueous-carbonic vapor. The Cl concentration of melts increases with the Cl contents of the fluid unless the melt coexists with vapor plus hydrosaline liquid at fixed pressure and temperature; this phase assemblage buffers the Cl content of each phase with increasing Cl in the system. The Cl content of fluid(s)-saturated melts is independent of the CO_2 concentration of the saline liquid ± vapor with up to 21 wt% CO_2 in the fluid(s). The experiments show that Cl dissolution in aluminosilicate melts increases with temperature and pressure. Chlorine solubility is also a function of melt composition; it increases with the molar $([Al^{1/2}+Ca^{1/2}+Mg^{1/2}+Na]/Si)$ of the melt.

These experimental data have been integrated with results involving 41 other experiments (Webster and De Vivo 2002) to develop a broadly expanded model that supports calculation of Cl solubility in 163 aluminosilicate melts. This empirical model applies to Cl dissolution in melts of most silicate magmas at depths as great as 25 km. It determines the exsolution of hydrosaline liquid, with or without a coexisting vapor, as magmas ascend from depth, cool, crystallize, and differentiate from mafic to felsic compositions. In combination with H_2O solubility models, our model supports determination of H_2O-Cl solubility relations for most aluminosilicate magmas and is useful for barometric estimations based on silicate melt inclusions containing low CO_2 and moderate to high Cl concentrations.

The model is applied to the phase relations of fluids in volatile-enriched magmas of Augustine volcano, Alaska. The Cl and H_2O concentrations of melt inclusions from 14,

basaltic to dacitic eruptive units are compared with modeled solubilities of Cl and H_2O in Augustine melts. The majority of these eruptions involved magmas that first exsolved aqueous to aqueous-carbonic vapors when the melts were dacitic in composition (i.e., before the residual melts in these magmas had evolved to felsic compositions) and well prior to the eruptions. Hydrosaline liquid with or without a vapor phase exsolved from other, more-felsic fractions of Augustine melts at low, near-surface pressures of several tens of bars.

Keywords: Hydrothermal experiments, chlorine solubility, brine, rhyolite melt, basalt melt, melt inclusions

INTRODUCTION

Chlorine is one of the five primary volatile components (e.g., H_2O, CO_2, S, Cl, and F) that dissolves in magmas (Carroll and Webster 1994); some magmatic fluids and volcanic gases are strongly enriched in Cl. The presence of the chloride ligand controls the dissolution of numerous ore metals in fluids of mineralizing magmas, and in particular, the HCl component in magmatic gases is key to processes of hydrothermal metasomatism and metal transport occurring in and around plutons and overlying volcanic edifices.

The impact of Cl in these magmatic and mineralizing processes varies with its concentration in natural melts and is also a function of how Cl partitions between melts, fluids, and minerals during magma differentiation (Metrich and Rutherford 1992; Shinohara 1994; Signorelli and Carroll 2000; 2002; Carroll 2005; Webster and Mandeville 2007; Shinohara 2009). Analyses of silicate melt inclusions (MI) indicate that maximum Cl concentrations approach 0.9 wt% for subduction-related, mafic to felsic arc magmas; 0.6 wt% for evolved continental rhyolite-forming magmas, and far less, only 0.04 wt% for MORB magmas (Aiuppa et al. 2009). Interestingly, terrestrial peralkaline magmas may dissolve more than 1 wt% Cl

(Aiuppa et al. 2009), and interpretation of geochemical relationships implies that some Martian magmas may also be highly enriched in Cl (Filiberto and Treiman 2009).

The exsolution of magmatic Cl-bearing vapor with or without a Cl-enriched hydrosaline liquid from melt (Fig. 1), and the partitioning of Cl between melt-fluid(s), melt-apatite, melt-biotite, and melt-amphibole are controlled by the solubility of Cl in melts. Chlorine speciation and dissolution in silicate melts are poorly understood. Experiments, analyses, and modeling do indicate that Cl speciates with alkalis in melts and that the influence of Cl on melt viscosity and rheology varies with the aluminosity and alkalinity of aluminosilicate melts (Stebbins and Do 2002; Chevychelov et al. 2003; Sandland et al. 2004; Stagno and Dolejs 2008; Baasner et al. 2013). Few volatile solubility models address the solubility behavior of Cl in magmas. The volatile partitioning model of Witham et al. (2012) is innovative in that it is the first to include the behavior of Cl in COHSCl-bearing fluids versus that in basaltic melts, but it is limited only to mafic melts. The empirical model of Webster and De Vivo (2002) covers Cl solubility for a wide range of melt compositions. This model, however, only applies to a single pressure, and its supporting experiments involve a range of temperatures without actually accounting for the influence of temperature on Cl solubility.

We have conducted 121 new hydrothermal experiments to determine the solubility of Cl in rhyolitic to basaltic melts. The influences of pressure, temperature, and melt and fluid composition on Cl dissolution in aluminosilicate melts are addressed in the description of results that follow. These new experimental data are integrated with results of 41 runs of Webster and De Vivo (2002) to develop an expanded Cl solubility model that applies to most geologically relevant, aluminosilicate melts at pressures (P) of ca. 1 bar to 7000 bars and temperatures (T) of 700-1250°C. This new empirical model is tested against Cl solubility data

from other, prior experimental studies (Metrich and Rutherford 1992; Signorelli and Carroll 2000; Chevychelov et al. 2003; Botcharnikov et al. 2004; 2007; Chevychelov et al. 2008; Beermann 2010), and the agreement is quite good. The model is also used to identify and interpret the compositions, timing, and behavior of Cl-enriched fluids for the volatile-charged magmas (Symonds et al. 1990) of Augustine volcano, Alaska.

Nomenclature

In this report, we define fluids as volatile-bearing, polycomponent, non-crystalline phases. We treat vapor as a relatively low-density fluid phase that is dominantly aqueous or aqueous carbonic in composition. Higher-density fluid phases in our experiments include silicate melt and various liquids. Specifically, melt refers to the highest-viscosity, aluminosilicate-dominated fluids addressed herein, and we consider hydrosaline liquid (HSL, also known as brine) to refer to electrolyte-enriched aqueous or aqueous-carbonic fluid. Fluid unmixing involves either the condensation of HSL from vapor or immiscible separation of vapor from HSL through boiling at sub-solvus *P*-*T*-composition conditions (Fig. 1). At shallow-crustal pressures and magmatic temperatures, Cl-bearing aqueous and aqueous-carbonic fluids unmix when the activity coefficients for H_2O and alkali chloride compounds exceed unity (Webster and Mandeville 2007). The solubility of Cl was determined for silicate melts, saturated in HSL with or without a coexisting vapor phase, as the maximum Cl concentration measured for each melt composition as a function of pressure, temperature, and fluid composition. For melts saturated in vapor (and no HSL), the maximum Cl concentration of the melt is controlled by the partitioning of Cl between melt and vapor.

The data presentation and discussion involve wt% or molar quantities. The molar abundance of certain components was computed as the ([wt% component/molecular or atomic weight of that component] in 100 grams of silicate melt).

METHODS

Experimental

All experiments were conducted with 2-8 mg of the chloride salts: NaCl ± KCl ± $PtCl_2$ ± $PtCl_4$ ± $CaCl_2 \cdot 2H_2O$ ± $MgCl_2 \cdot 6H_2O$ ± $FeCl_2 \cdot 4H_2O$ and 30-80 mg of finely ground natural and/or synthetic aluminosilicate glass powders in the starting charges (Table 1). The bulk compositions of the starting powders are listed in Table 1. A few runs also included 0.5-5 mg of H_2O ± NaF ± H_3PO_4 ± Fe_3O_4 ± $C_2H_2O_4 \cdot 2H_2O$ ± Durango apatite. Most experiments were conducted in 1-3 cm long, 3-5 mm diameter Au, $Ag_{70}Pd_{30}$, $Au_{90}Pd_{10}$, or $Au_{80}Pd_{20}$ capsules. The majority of the starting charges, to which hydrous chloride salts were added, were preheated at 400-500°C for at least one hour to reduce the quantity of H_2O adsorbed to the powders and salts before the capsules were crimped and sealed by welding. It was necessary to heat the open starting charges for runs conducted at ca. 1 bar to higher *T* of 600°C for at least 24 hours to remove as much H_2O as possible prior to sealing the capsules. These capsules were repeatedly heated and weighed until the mass change (i.e., mass decrease) was negligible. Afterward, all capsules were welded with either graphite or tungsten probes.

The ca. 1-bar runs required use of 7-8 cm long precious metal capsules. The additional capsule length was necessary to provide space for the excess volume occupied by the trace gases generated during the run as well as that of the air (present in the starting charges) at run *T*.

These experiments were conducted at ca. 700-1250°C and 1-7000 bars. All ca. 1-bar runs were conducted in one-atmosphere furnaces at the American Museum of Natural History (AMNH), and all other runs were conducted in internally heated pressure vessels (IHPVs) at either the AMNH or the Leibniz University of Hannover, Germany (LUH). At the AMNH, *T* was monitored in the IHPV with two chromel-alumel thermocouples spanning the length of the run capsules, and the *T* difference between the two thermocouples was 2-20°C for most runs. Argon run *P* was determined with factory-calibrated, Heise bourdon-tube-based gauges, and a recent calibration returned errors of ± 0.002 bars for pressures > 700 bars. All runs were quenched isobarically, and quench times to the glass transition *T* were generally < 30 seconds. Most AMNH runs were conducted at the ambient f_{H2} of the IHPV which imposes log f_{O2} of ca. NNO (i.e., the Ni-NiO oxygen buffer assemblage) to NNO+1.5 for geologically relevant pressures, temperatures, and water activities; additional details on f_{O2} for this IHPV are given in Webster and De Vivo (2002).

Five experiments, involving 26 individual run capsules, were conducted at the LUH. For these experiments, *T* was measured with four unsheathed S-type (Pt–$Pt_{90}Rh_{10}$) thermocouples that supported *T* control for the run capsules situated in the 3 cm-long hot zone. The precision on the reported run *T* is ± 10 °C; this accounts for the *T* gradient along the sample and for fluctuation of *T* during the experiments. Run *P* was monitored with a calibrated digital manometer having an uncertainty of about 10 bars, and the variation of *P* during the experiments was ≤ 50 bars. The Hannover IHPV was pressurized with argon and the experiments were performed at the intrinsic f_{H2} of the vessel. The f_{O2} within the capsules was controlled by the f_{H2} and f_{H2O} through the equilibrium reaction $H_2+½O_2↔H_2O$. For reference, the f_{O2} within capsules containing H_2O-saturated melts (pure H_2O fluid) was found to be close

to the f_{O2} of the NNO buffer + 2.6 log units during other, prior experimental studies with this apparatus (Schuessler et al. 2008). In order to avoid possible non-equilibrium quench effects, the samples were cooled rapidly at the end of the run by dropping the capsules into the cold part of the vessel (Berndt et al. 2002); the resulting rate of cooling is about 150 °C/second (Benne and Behrens 2003).

Electron Probe Microanalysis (EPMA)

The compositions of all experimental glasses were measured with wavelength-dispersive spectrometry using a Cameca SX-100 electron microprobe at the AMNH. Multiple analyses of run-product glass (e.g., 4-12) were performed to check for compositional homogeneity and obtain representative averages. Glasses were analyzed using distinct two-step protocols. Raw x-ray intensities from both steps of the protocols were reintegrated prior to calculating concentrations. Glasses were analysed as follows: Na, K, Fe, Si, and F in the first instrument pass using an accelerating potential on the beam of 15 kV and a 2-nA cup current; and Al, Ti, Ca, Mg, Mn, P, Cl, and S in the second instrument pass using an accelerating potential on the beam of 15 kV and a 10-nA cup current. Both beam conditions used a 5- to 10-µm, defocussed spot, and the glasses were moved continually under the electron beam to minimize alkali and/or F migration or loss during analyses. The H_2O concentrations of some run-product glasses (i.e., the melts) and melt inclusions were estimated with the by-difference method (i.e. [100 wt% - the EMPA total for glass analyses = estimated wt% H_2O in melt]).

The accuracy of EPMA was tested for Cl (Fig. 2) by analyzing a natural obsidian (the Big Southern Buttes [BSB] glass of MacDonald et al. [1970]), reagent-grade NaCl (containing 60.7 wt% Cl), reagent-grade KCl, a natural scapolite, and three synthetic apatites (Schettler et al. 2011) with this approach. The curve (Fig. 2) represents the 1:1 correspondence line for both

variables. Fitting the data with a line returns an R^2 of fit of (0.9998), so this analytical protocol is extremely accurate over a large range in Cl contents for the glasses and minerals.

The BSB glass (Macdonald et al. 1970) was analyzed during each analytical session to check for instrumental drift during the course of the investigation. The resulting uncertainties expressed as 1σ variability about the means for 52 analyses of the felsic BSB glass are: < 6 rel% for Cl, Na_2O, SiO_2, Al_2O_3, and K_2O (the BSB contains 0.2, 4.27, 75.1, 12.3, and 4.6 wt% of these constituents, respectively); 8-37 rel% for F, FeO, CaO, and TiO_2 (BSB contains 0.31, 1.55, 0.48, 0.09 wt% of these constituents, respectively); and 58-140 rel% for the trace components MnO, MgO, and P_2O_5 (the BSB contains 0.04, 0.004, 0.004 wt% of these constituents, respectively).

RESULTS

Characteristics of experimental run products

The products of the experimental runs include variably vesicular glass; oxide, phosphate, and silicate minerals; and traces of salts (Table 1). The vesicles contain combinations of saline aqueous liquid, vapor, salt crystals, and silicate minerals.

Achievement of melt-fluid(s) phase equilibria for these P-T-X conditions

The interaction of the silicate melts with the various chloride salts, at *P* and *T*, involves the dissolution of salt-sourced cations and Cl ± H_2O ± CO_2 into the melts and the exchange of cations and other melt-sourced aluminosilicate components between the melts and starting fluid(s). Achievement of chemical equilibrium between these phases requires sufficient time for the delivery of Cl to the melt, the diffusion of Cl throughout the melt, and for the movement of the most slowly diffusing cations through melt for exchange with the fluids. We note that $PtCl_2$ and $PtCl_4$ can be employed as chloride sources for hydrothermal experiments, but they

should be used with caution. We assume that these salts interact primarily with the trace H_2O adsorbed to the solid components in the starting charges, and they break down to form HCl during the experimental run up to *T* and *P*:

$$2PtCl_2 + 2H_2O = 2Pt° + 4HCl_{fluid} + O_2 \quad (1)$$

$$PtCl_4 + 2H_2O = Pt° + 4HCl_{fluid} + O_2 \quad (2)$$

where Pt° refers to platinum metal. It follows from these reactions that HCl contains the highest Cl concentration (i.e., 97.3 wt% Cl) of the various chlorides used in the starting charges. Moreover, HCl contains no cations other than protons so this chloride source requires significant diffusion and partitioning of cations out of the melt and to the HSL ± vapor in order for all phases to equilibrate at run conditions. It follows that short run durations and a lack of equilibrium could involve artificially high, apparent Cl solubilities in the silicate melts because of the high initial Cl contents of the HCl-enriched fluids generated by $PtCl_2$ and $PtCl_4$. This is likely because the Cl concentrations of the fluids, prior to equilibrium, would remain artificially high until Na, K, Ca, Mg, and other cations were taken up into the fluids. The exchange of these cations for H dilutes and reduces the Cl contents of the fluids. Our experiments involved extended run durations; most were conducted for 120 hours and some for up to 525 hours. Given the internal consistency of the data (addressed below), our runs are considered to represent equilibrium conditions.

Alternatively, the chloride source may interact with iron:

$$3PtCl_2 + 6FeO = 3Pt° + 2FeCl_3 + 2Fe_2O_3 \quad (3)$$

or as:

$$PtCl_4 + 4Fe^{2+}_{silicate\ melt} = Pt° + 4Fe^{3+}_{silicate\ melt} + 4\ Cl^-_{silicate\ melt} \quad (4)$$

This is a preprint, the final version is subject to change, of the American Mineralogist (MSA)
Cite as Authors (Year) Title. American Mineralogist, in press.
(DOI will not work until issue is live.) DOI: http://dx.doi.org/10.2138/am-2015-5014

and modify the ferric/ferrous iron ratios of the melts. Given that these reactions involve changes in the ferric/ferrous ratios, they will be influenced by f_{O2} and, hence, on the intrinsic f_{H2} of the experimental equipment and the a_{H2O} in the system. Reactions (3) and (4) are more likely to occur in iron-enriched runs with comparatively low a_{H2O} since reactions (1) and (2) require H_2O to react with the platinum chloride salts to form HCl .

The phase relations of HSL ± vapor for NaCl-H_2O, KCl-H_2O, and KCl-NaCl-H_2O systems are well established (Bodnar et al. 1985; Chou 1987; Driesner and Heinrich 2007), but the influence of Mg, Fe, Ca, and other cations on electrolyte phase equilibria are poorly established for the ranges of *P* and *T* of this study. Herein, we use the phase relations of the compositionally simple NaCl-H_2O system to determine the presence of vapor, HSL, or HSL ± vapor in our experiments. Mass balance calculations indicate that the Cl concentrations of the bulk, integrated fluids in these experiments ranged from 30 to > 60 wt%. These values are consistent with the presence of HSL plus vapor or HSL only in our runs.

Influence of temperature on Cl solubility in melt

Chlorine solubility in aluminosilicate melts, that are HSL ± vapor saturated, increases with *T*. To determine the influence of *T* on Cl dissolution in silicate melts, it is necessary to extract and plot solubility data for fixed melt composition and fixed *P* conditions, because of the complex interrelationships between Cl solubility and *T*, *P*, and composition (Fig. 3). For example, the concentration of Cl in rhyolitic melts saturated in HSL at 2000 bars increases by 50 rel% as *T* increases from 700 to 1150°C. Similarly, the Cl contents of HSL- ± vapor-saturated phonolitic melts at 5000 bars increase by 17 rel% as *T* increases from 1050 to 1250°C.

Few, prior experimental studies have addressed the influence of *T* on Cl dissolution in melts that are saturated in an HSL ± vapor. Published results primarily involve the partitioning of Cl between aqueous vapor and melts. Stelling et al. (2008), for example, did not detect a clear influence of *T* varying from 1050-1250°C on Cl solubility in fluid-saturated, molten Mt. Etna basalt at 2000 bars, and Chevychelov et al. (2008) saw no change in D_{Cl} (Cl content of aqueous vapor ± HSL/Cl content of silicate melt) for phonolitic melts between 850-1000°C at 2000 bars. Conversely, Webster (1992b) observed D_{Cl} decreasing (less Cl in fluids and more Cl in melt) with increasing *T* for haplogranite melts at 2000 bars. This is consistent with the results of the present study.

Influence of pressure on Cl solubility in melt

The molar Cl solubility in melts (i.e., expressed as the moles of Cl in 100 grams of silicate melt), that are saturated in HSL ± vapor, also increases with *P*. Figure 4 shows how *P* affects the dissolution of Cl in melts ranging from F-enriched topaz rhyolite to basalt. Chlorine solubility, however, varies strongly with differences in Ca and Mg contents, and concentrations of MgO and CaO differ significantly from rhyolitic to basaltic melts. Consequently, we have normalized the measured Cl concentrations in melt to equivalent molar concentrations of (Ca + Mg), in order to isolate the influence of *P*. Basaltic and latitic melts show the smallest influence of *P* on Cl solubility; whereas, the phonolitic and topaz rhyolitic melts show the strongest influence of *P*. Each data set involves small to modest differences in *T* as well. Hence, we have corrected the molar (Cl/Ca+Mg) measured for the topaz rhyolitic melt at 703°C to the value expected at 1000°C (given the Cl solubility versus *T* relations of Figure 3) to be more consistent in *T* to the other runs involving this melt composition. Regarding the phonolitic melts, we have included but also highlighted the two lowest-*T* runs conducted at

1000 and 1050°C, which are offset to Cl contents below the curve for all other runs conducted at 1166-1250° C. These comparatively lower Cl solubilities are consistent with the influence of *T* on Cl dissolution in melt (Fig. 3). For each melt composition, the Cl solubility in melt increases with increasing *P*. The positive correlation, observed between Cl dissolution in melts and *P* in this study, has been determined previously with a variety of HSL- ± vapor-saturated melts (Malinin et al. 1989; Webster 1992a;b; Webster and Rebbert 1998; Webster et al. 1999; Webster et al. 2003; Webster 2004; Stagno and Dolejs 2008).

It is useful to compare these observations with those of published experimental investigations, but interpreting the disparate results can be challenging because of the competing influences of *P*, *T*, and composition on Cl dissolution. Chevychelov and Suk (2003), for example, observed their maximum Cl concentrations in basaltic, dacitic, albitic, and orthoclasitic melts at 1000 bars and 1250°C; whereas, they determined comparatively lower Cl contents in these melts at $P < 1000$ bars but also at higher *P* (i.e., 3000 bars). Alletti et al. (2009) observed decreasing D_{Cl} in experiments with Etna basalt as *P* increased from 10-2000 bars. It is noteworthy that the relationship involving the maximum Cl concentration of a melt and *P* is diametrically different for vapor-saturated melts and for some melts saturated in vapor plus HSL (Carroll 2005). In contrast to that determined, herein, i.e., that maximum Cl concentration of melts increases with *P*, others have concluded that the concentration of Cl in silicate melts increases with decreasing *P* for melts saturated in vapor or vapor plus HSL at shallow-crustal *P* (Shinohara et al. 1989; Shinohara 1994; Metrich and Rutherford 1992; Chevychelov and Chevychelova 1997; Signorelli and Carroll 2000; 2002). In addition, as discussed below, the a_{H2O} and a_{Cl} in the system can be fixed as the bulk concentrations of H_2O

and Cl vary at constant *P* and *T* if both fluid phases are stable with melt (Shinohara et al. 1989; Lowenstern 1994; Webster and Mandeville 2007).

Influence of melt composition on Cl solubility

The extent to which Cl dissolves in silicate melts varies dramatically with composition (Fig. 5). Chlorine solubility increases strongly as the silica content of melt decreases (Kotlova et al. 1960; Iwasaki and Katsura 1967), and hence, it follows that the Cl contents of melts increase as other cations (e.g., Ca, Mg, Na, Fe, F, and K) are added to molten silica (Webster and De Vivo 2002; Chevychelov and Suk 2003). It has also been determined, however, that Cl solubility increases with reduced concentrations of titanium and phosphorus in melt (Webster and De Vivo 2002). In general, Cl solubility can decrease by more than an-order-of magnitude as HSL-saturated melts evolve from basalt to rhyolite.

Our results are consistent with those of prior experiments demonstrating the fundamental influences of the molar A/CNK ($Al_2O_3/(CaO+Na_2O+K_2O)$), N/NK ($Na_2O/(Na_2O+K_2O)$), and (Ca+Mg)/(Na+K) ratios of melts on the efficiency of Cl dissolution at fixed *P* (Metrich and Rutherford 1992; Chevychelov and Chevychelova 1997; Signorelli and Carroll 2000). Following on these relationships, we have compared the Cl solubility of HSL- ± vapor-saturated melts with increasing moles of ($Ca^{1/2}+Mg^{1/2}+Al^{1/2}+Na$) and decreasing moles of Si for a range of pressures and temperatures (Fig. 6). Potassium is not included given its significantly smaller control on Cl than those of these cations (Webster and De Vivo 2002). The square-root relationships applied to the multivalent cations were determined empirically, by the best degree of fit to these data. The cause of the apparent square-root relationship is undetermined, but it may simply reflect how (+2)-charged cations associate with (-1)-charged chloride ions dissolved in the melts.

Characteristics of the fluids of these experiments

The HSL, with or without vapor, constituting the fluids in most of these experiments, consisted primarily of Cl^-, H_2O, Na^+, K^+, Ca^{2+}, Fe^{2+}, Fe^{3+} and H^+. The dominance of these ions in such brines is supported by observations from prior experiments and theoretical considerations (Kilinc and Burnham 1972; Webster et al. 2009; Shinohara 2009; Beermann 2010; Zajacz et al. 2012). At the pressures and temperatures of this study, these cations and H^+ form chemical complexes with the chloride ion, and the stable chloride species vary with changes in *P*, *T*, fluid density, and chloride activity. In these experiments, the C and S concentrations of the starting charges of most runs were too low to generate influential abundances of CO_2, CH_4, SO_2, or H_2S in the HSL.

Four of the experiments, involving phonolitic and haplogranitic melts at 2000 bars, included CO_2 added to the starting charges as oxalic acid. The concentrations of CO_2 in the HSL ± vapor were calculated by mass balance, using methods of Webster et al. (2009), and they ranged from 8 to 21 wt% at run conditions. It is likely that these CO_2-enriched experiments included vapor in addition to the HSL because the CO_2 contents exceed the CO_2 solubilities that were determined for H_2O-NaCl-CO_2 brines at magmatic pressures and temperatures (Heinrich 2007). All CO_2 not soluble in the melt and HSL would force the exsolution of an aqueous-carbonic vapor phase (Bowers and Helgeson 1983). Comparison of the measured Cl concentrations in these melts with those of CO_2-deficient, phonolitic and haplogranitic equivalents shows no detectable differences in Cl solubility.

DISCUSSION

Development of an expanded, empirical chlorine solubility model

The solubilities of Cl determined for the 121 Cl-saturated silicate melts of this study are consistent with those of 41 experiments conducted previously (Webster and De Vivo 2002). The latter Cl-enriched experiments were run at ca. 2000 bars with *T* ranging from 786-1193°C. The effect of *T* on Cl solubility was not addressed by Webster and De Vivo (2002); rather, the primary focus of their study was to determine relationships between melt composition and Cl dissolution and to generate a Cl-solubility model applicable to a wide compositional variety of silicate melts at fixed *P*. Their model was based on association coefficients, relating Cl to specific ions in the melt, that correlate with Cl solubility. Increasing concentrations of Mg, Ca, Na, Fe, K, Al, and F and decreasing concentrations of titanium and phosphorus were observed to correlate with increasing Cl solubilities in melt. The individual cation-Cl correlations may or may not represent chloride species present in the melts. The Webster and De Vivo (2002) model also addressed the influence of differing melt aluminosity and alkalinity on Cl solubility.

For the present study, we have combined the two sets of data, and this larger integrated set of 163 experiments is used to support an expanded Cl-solubility model (Appendix). This new model involves several refinements to the compositional terms applied by Webster and De Vivo (2002) in their isobaric model; for example, it better accounts for the influence of the (Na/(Na+K)) ratio of alkaline melts than the original model. The expanded model also accounts for effects of changing *P* and *T*. Hence, it predicts Cl solubility for most geologically relevant melt compositions for OHCCl-bearing magmas at near-surface temperatures and depths and to magmas at depths as much as 25 km below surface.

Comparison of the calculated Cl contents of the melts with the measured experimental values shows good correspondence for most runs (Fig. 7A). The inaccuracy or error on the modeled Cl abundances is ≤ 10 rel% for the majority of the experiments, and all but 16 of the

runs have calculated Cl concentrations within 20 rel% of the measured Cl contents. In this figure we have highlighted the Cl contents of the 4 CO_2-added experiments. The modeled Cl solubilities for the CO_2-bearing melts lie within the ± 10 rel% error curves applied to all data. Thus, the addition of CO_2 has little measurable impact on Cl solubility in HSL-saturated melts which is consistent with prior research. Botcharnikov et al. (2007), in their experimental study focused on the dissolution of OHCCl-bearing fluids in andesitic melts at 1050 and 1200°C and 2000 bars, determined that the concentrations of Cl dissolved in andesitic melts are not "considerably affected" with up to 35 wt% CO_2 in the fluid(s) (Fig. 7B). Similarly, an investigation of OHCSClF-bearing fluid(s) dissolving in phonolitic melts at 2000 bars determines no detectable influence of up to 40 wt% CO_2 in fluids on Cl dissolution in the coexisting melts (Webster et al. in review). It should be kept in mind, however, that if the addition of CO_2 results in vapor saturation of the melt and HSL, then thermodynamically one should expect some (potentially subtle) change in the Cl solubility relations due to the phase change induced on the system.

The expanded Cl model does have limitations. It does not account for varying ferric/ferrous ratios of silicate melts. As explained, the experimental equipment generates log $f_{O2} \geq$ (NNO). We could not, however, determine the effect of $(Fe^{2+}/(Fe^{2+}+Fe^{3+}))$ on Cl solubility since the ferric-ferrous contents of the melts were not determined, but we assume that the iron was largely oxidized based on the relevant f_{O2}. Recent work does show strong relationships between Cl and Fe^{2+} and Fe^{3+} for fluid-absent (Webb et al. 2014) and fluid-saturated mafic melts (Bell and Simon 2011). Also, the expanded model does not account for the influence of oxidized S species dissolved in melts and fluids. Prior experimental investigations determine that the solubility of Cl in silicate melts decreases substantially with

increasing S under generally oxidizing conditions (Botcharnikov et al. 2004; Webster et al. 2009). As addressed below, the addition of S to fluid-saturated basaltic, phonolitic, trachytic, dacitic, and rhyodacitic melts reduces Cl solubility with f_{O2} > NNO.

To test the expanded model, we have calculated Cl solubilities in melt compositions of prior experimental studies (Metrich and Rutherford 1992; Signorelli and Carroll 2000; Chevychelov et al. 2003; Botcharnikov et al. 2004; 2007; Chevychelov et al. 2008; Beermann 2010) and compared these solubilities with the maximum Cl concentrations measured in these experiments (Fig. 7B). The comparison shows good agreement with the HSL-saturated granitic, granodioritic, phonolitic, andesitic, and basaltic melts of the prior work. The modeled Cl concentrations are equivalent to the measured equivalents in the run-product glasses within the analytical accuracy of the model.

Modeled Cl-H_2O solubility curves and their applications to magmatic systems

The phase equilibria of melts saturated in HSL and vapor exert fundamental controls on the chemical behavior of H_2O and Cl (shown schematically in Fig. 1 and Fig. 8A). These controls include buffering of the thermodynamic activities of H_2O and Cl in the melts and coexisting, immiscible vapor plus HSL even as the H_2O/Cl of the bulk system changes. At *P*-*T*-composition conditions near but not within that of the vapor-HSL solvus (Fig. 8B) (i.e., with insufficient Cl for stable HSL or with insufficient H_2O for stable aqueous vapor - so only one fluid is present) or at conditions within the solvus, H_2O and Cl exhibit strongly non-ideal volatile mixing behavior. This is expressed graphically for dacitic melt saturated in one or more fluids in Figure 8A and for the melt-absent H_2O-NaCl system in Figure 8B. The concentration of H_2O in this melt remains constant from points [3] to [4] (in the vapor field, outside of but near the vapor-HSL solvus) with increasing Cl in the bulk system. At invariant

point [4] in Figure 8A (relating to subsolvus *P-T*-composition conditions in Fig. 8B), vapor coexists with HSL and the activities of H_2O and Cl in all phases are fixed with continued addition of Cl to the system (as long as the system remains at this point), because the activity coefficients for these volatiles vary progressively to offset the increasing fraction of Cl (Webster and Mandeville 2007). Similarly, with increasing Cl in the H_2O-NaCl system (Figure 8B) the H_2O and NaCl concentrations of the vapor and HSL are fixed while the ratio of (vapor/HSL) decreases. From points [4] to [5] (in the HSL field at near-solvus conditions) the concentrations of H_2O decrease and the Cl contents remain fixed in the melt with addition of Cl. We also note, however, that prior analysis of conditions like these by Shinohara (1994) suggests that the Cl concentration of the melt may increase somewhat from points [4] to [5].

Volatile behavior is different, however, for systems characterized by a single fluid phase. In such systems at near-solvus conditions (i.e., outside of the vapor-HSL solvus from points [1] to [2] along the curve of Fig. 8A and for the melt-free NaCl-H_2O system in Fig. 8B), the melt coexists with a single fluid phase throughout the full compositional range. The fluid evolves progressively from an H_2O vapor to chloride-dominated HSL with increasing Cl in the bulk system.

Fractional crystallization leads to increasing concentrations of H_2O and Cl in residual melt, but fluid phase separation may control the activities of H_2O and Cl in natural melts during magma evolution. For cooling and crystallizing felsic magmas at *P*-T-composition conditions at or near that of the relevant minimum melting point, melt evolution in the presence of vapor and HSL may fix or buffer the activities of H_2O and Cl in the residual melt and fluid phases due to the phase constraints addressed above. Details of these relationships have also been

discussed for experimental and natural systems by Shinohara (1994), Lowenstern (1994), Candela and Piccoli (1995), and Webster (2004).

With this new model for Cl and using extant H_2O solubility models, one can generate mixed H_2O-Cl solubility curves for aluminosilicate melts that are applicable to melt-, vapor-, and HSL-bearing magmas at shallow-crustal pressures and temperatures like those in Figure 8A. The maximum Cl concentration in the melt (point [5], Fig. 8A) is computed with the expanded Cl solubility model of the present study, and the melt's saturation H_2O concentration (point [3], Fig. 8A) is calculated from any of the many published models on H_2O solubility for the specific pressure-temperature-composition conditions of interest (e.g., Burnham 1997; Moore et al. 1998; Papale 1999; Newman and Lowenstern 2002; Moretti et al. 2003; Liu et al. 2005). For systems comprised of coexisting vapor and HSL, the Cl and H_2O solubilities in melt are graphically linked with horizontal and vertical lines like those in Figures 1 and 8. Conversely, for magmas at higher *P*, at which a single fluid is stable for widely varying (Cl/H_2O) in the melt, the fluid solubility curves are more like that linking points [1] and [2] because the activity-composition, mixing relationships for H_2O and NaCl vary strongly with *P*. Shmulovich and Graham (1996) provide details on how these curves vary with *P* and fluid composition.

Applications to degassing of volatile-enriched magmas of Augustine volcano, Alaska

Augustine is an island-arc volcano situated 290 km from Anchorage, Alaska. Augustine has commercial significance in this region because it lies near trans-Pacific polar routes that pass through Anchorage airport. Air traffic has been impacted by its eruptive activities. Augustine last erupted in 2006 and has erupted at least six other times in the last 200 years (Power and Lalla 2010). Augustine emits Cl-enriched volcanic gases (Symonds et al. 1990)

and low-K, calc-alkaline magmas. Melt inclusions suggest that intermediate to felsic fractions of Augustine melts contain up to 8 wt% H_2O, 1 wt% S, 0.78 wt% Cl, 0.5 wt% F, and 0.14 wt% CO_2 (Johnston 1978; Tappen et al. 2009; Roman et al. 2006; Webster et al. 2010; Larsen et al. 2010). Most of the analyzed intermediate to felsic MI, however, contain less than 300 ppm CO_2. All MI discussed herein were hosted by olivine, plagioclase, pyroxenes, or amphibole, and the MI were glassy with small vapor/shrinkage bubbles (i.e., these data have been filtered for leaked or otherwise flawed MI by the various authors before publication).

We have calculated Cl-H_2O solubility relations to interpret degassing processes of Augustine magmas (Fig. 9). This approach requires constraints on the bulk compositions of the melts and their pressures and temperatures. Hence, we apply the compositions of > 275 MI analyzed from 14 prehistoric and historic eruptive units ranging from basalt to dacite in bulk composition. The basaltic unit is the oldest among these. Field relations suggest that it is coeval with rhyolitic units (not addressed herein) dated at ca. 26,000 years (Coombs and Vasquez 2012). All other studied units are younger than 2200 years in age. The compositions of the MI are basaltic, basaltic-andesitic, dacitic, rhyodacitic, and rhyolitic. It is important to note, here, that prior interpretations of geochemical relationships involving these volatiles (Johnston 1978; 1979; Roman et al. 2006; Tappen et al. 2009; Webster et al. 2010) indicate that the felsic to intermediate-silica content MI sampled eruptions of Augustine magmas containing Cl-enriched vapor ± HSL that first exsolved these fluids well before the eruptions. Iron-titanium oxide-based geothermometry determines temperatures of crystallization for the felsic MI-bearing phenocrysts ranging from 780 to 970°C (Tappen et al. 2009; Roman et al. 2006; Webster et al. 2010; Larsen et al. 2010). For simplicity in the modeling, all rhyodacitic and rhyolitic MI (hosted primarily by plagioclase phenocrysts) are assumed to have been

trapped at *T* of 900°C, the dacitic MI (hosted primarily by pyroxene, plagioclase, and amphibole phenocrysts) at 1000°C, and the mafic MI (hosted by olivine and pyroxene phenocrysts) at 1100°C. Individual pressures of MI entrapment were calculated for each MI as follows. Actual H_2O concentrations were measured for a small number of these MI by Fourier-transform infrared spectroscopy (FTIR), but most were estimated with the EPMA water-by-difference technique (WBD). Given the interpretation that many of the felsic to intermediate MI represent fluid(s)-saturated magmas, approximate pressures of MI entrapment can be estimated by applying the apparent H_2O concentrations to H_2O solubility versus *P* relations calculated with the model of Newman and Lowenstern (2002). Moreover, for the sake of discussion, we plot only those felsic MI with apparent pressures of entrapment ≤ 2000 bars (for 900°) because the equilibrium phase relations should involve two stable fluid phases based on those of the system NaCl-H_2O (Bodnar et al. 1985; Chou 1987) at these *P*-*T* conditions and for the elevated Cl contents involved. The stability of coexisting vapor plus HSL is poorly constrained above 2000 bars. We assume that the WBD and FTIR H_2O concentrations in these glassy MI represent those of the basaltic to rhyolitic melts at the time of melt entrapment.

Fluid phase relations with OHCl±C-bearing basaltic to rhyolitic melts. We compare the Cl contents with the estimated H_2O concentrations of the MI from the 14 eruptive units (Fig. 9). We do not address the influence of CO_2 on the phase equilibria of Augustine magmatic fluids in detail because of the paucity of CO_2 measurements for these MI. However it is important to recall that the experimental observations of this and prior work (Botcharnikov et al. 2007; Webster et al. in review) indicating that Cl dissolution in CO_2-bearing melts saturated in vapor ± HSL does not vary significantly with the addition of up to 40 wt% CO_2 to the bulk

fluids. It follows that the Cl solubility relations discussed below will be independent of the CO_2 contents of Augustine magmas even though they are not formally addressed herein.

We have partitioned the Augustine MI data into 4 groups, with corresponding graphs, based on their differences in bulk composition and computed Cl solubilities. We estimated the (maximum) H_2O solubilities for each melt (MI) composition with VolatileCalc (Newman and Lowenstern 2002) and the Cl solubilities with the expanded model of this investigation. The computed Cl solubilities represented by the curves for the various *P* conditions (Fig. 9 A,B,C,D) are the maxima for the least-evolved MI composition in each group, and they bear on HSL- (± vapor-) saturated melts having compositions representative of each grouping of MI for the specified *T*.

Figure 9A shows MI of basalt and basaltic-andesite composition, and the apparent H_2O contents exhibit a wide range consistent with entrapment of the MI from vapor-saturated melts at 90 bars to $P > 2000$ bars. The volatile components of these MI do not support the presence of HSL in these mafic magmas. Figure 9B addresses Cl and H_2O behavior for somewhat more-chemically evolved, dacitic to rhyolitic MI that are characterized by Cl solubilities less than those of the mafic MI. Saturation of these melt compositions in HSL requires up to 1.2 wt% Cl at 2000 bars. Melt inclusions from 06AUMC008.p1 containing ca. 0.7 wt% Cl and 0.4 to 1 wt% H_2O are consistent with entrapment of HSL- and vapor-saturated rhyodacitic magma at *P* near 50 bars, and several other MI reflect trapping of similar magmas at lower *P*. In contrast, most other MI reflect entrapment of Cl-deficient vapor in magmas at *P* from < 50 bars to as much as 2000 bars, because saturation in HSL at 50 bars would require Cl contents exceeding most of the measured Cl concentrations for this set of MI. Figure 9C bears on MI that are marginally more evolved than those addressed in Figure 9B, and hence, the associated

maximum Cl solubilities are somewhat lower at ca. 0.9 wt% for 2000 bars. The concentrations of H_2O and Cl in these rhyodacitic to rhyolitic MI indicate that most were trapped at $P < 2000$ bars from vapor-saturated magma. In contrast, the 8 MI from samples 06AUCWM012, 06AUJW010, and 06AUJW004 located on or nearest to the doubly dotted line connecting the HSL plus vapor coexistence points for 25 and 2000 bars imply entrapment of HSL- and vapor-saturated magmas at P of 25 bars and higher but less than 2000 bars. The 06AUJW004 MI containing the lowest H_2O and Cl contents appears to have trapped from a vapor- ± HSL-saturated magma at a shallow-crustal P much lower than 25 bars. The most chemically evolved (i.e. all-rhyolitic) MI are shown in Figure 9D, and they bear on entrapment of vapor-saturated Augustine melts at ca. 15 up to 2000 bars. Here also, several MI reflect entrapment of HSL-bearing melts at near-surface P.

The variability in apparent H_2O concentrations of these MI groups reflects magmatic degassing processes occurring over a wide range of shallow-crustal entrapment $P < 2000$ bars. The Cl contents, on the other hand, show comparatively narrow ranges. These comparatively limited or fixed Cl contents reflect the influences of Cl partitioning between melt and vapor ± HSL in some portions of these magmas. These fluid phases were present as the magmas cooled and differentiated, and passed through shallow-crustal P during their ascent to the surface. Interestingly, the limited or buffered maximum Cl concentrations range from only 0.3 to 0.7 wt% for many of the dacitic to rhyolitic MI.

To further interpret degassing that was concurrent with magma evolution and ascent, we compare the measured Cl contents with the Larsen melt differentiation index (e.g., the wt%-based $[(K_2O) + (SiO_2)/3]-[(CaO) + (MgO) + (FeO)]$ of the MI (Fig. 10A). Although magma evolution at Augustine volcano has historically involved variable extents of magma mingling

and mixing (Roman et al. 2006; Larsen et al. 2010), for this discussion we address the differentiation of those fractions of fluid-saturated magma primarily affected by fractional crystallization with minimal magma mixing or mingling. In this figure, we also show (with an arrow) the predicted increase in Cl contents of melts evolving from basaltic to rhyolitic compositions with no fluids or minerals present to sequester volatiles from melt (i.e., the arrow treats these volatiles as incompatible melt components). The Cl concentrations and change in Larsen index were computed from mass-balance-based modeling of fractional crystallization of a melt having a composition equivalent to those of the MI sampled from the 26,000-year old basalt. Most of these mafic MI contain: 2-6 wt% H_2O, 0.6-1.1 wt% SO_2, 0.3-0.45 wt% Cl, and 40-400 ppm CO_2 (Zimmer 2010; Webster unpublished data). The compositions of plagioclase, amphibole, pyroxene, accessory phases ± olivine used in the fractional crystallization modeling were derived from prior petrologic investigations of Augustine eruptive units (Roman et al. 2006; Tappen et al. 2009; Webster et al. 2010; Larsen et al. 2010). This approach assumes the basaltic magmas that supplied the eruptions occurring in the past 2200 years had similar bulk compositions and volatile contents as those of the ca. 26,000-year old mafic MI used herein.

Comparison of the MI data with the modeled differentiation relations shows that as the magmas differentiate, under closed-system conditions with no stable fluids present, the expected Cl contents in the fractions of residual melt exceed those measured in all of the dacitic MI and are also greater than those in most of the rhyolitic MI. We interpret this difference in Cl contents to indicate that an aqueous vapor (or, potentially, an aqueous-carbonic vapor given the tens to low hundreds of ppm CO_2 in the assumed mafic starting melt composition) had exsolved from most of the magmas supplying the 2100 years before present

(ybp) and younger eruptive units prior to or at the dacite stage of melt evolution. In this regard, the most-volatile enriched basaltic fractions of melt would have exsolved H_2O- and CO_2-dominated vapor at pressures (and equivalent depths) of several kilobars.

We also interpret the fluid-phase relations as a function of melt evolution with this approach, and Figure 10B compares the actual versus modeled Cl concentrations for the MI. This figure includes an arrow expressing the expected increase in Cl content of residual melt fractions (based on mass-balance modeling of 50% fractional crystallization of olivine, plagioclase, pyroxenes, amphibole, iron-titanium oxides, and apatite from melt), as the melts evolve from basalt to rhyolite with no fluid(s) stable, versus the calculated (maximum) solubility of Cl for the modeled bulk melt compositions represented by the arrow in Figure 10A. Figure 10B also includes the 1:1 correspondence curve (dashed) for measured versus calculated Cl concentrations of the melts. This curve represents the Cl concentrations in melt that require saturation in HSL ± vapor; no data should lie above this curve (i.e., accounting for the associated errors in accuracy of the expanded Cl solubility model) if the calculated Cl solubilities were based on accurate pressures and temperatures for each MI. Regarding the influence of potentially inaccurate *P* and *T* estimates, changing the assumed *T* by 100°C or assumed *P* by 1000 bars causes the modeled Cl solubility to vary < 10 rel%.

Comparison of the actual versus predicted Cl contents of these MI in light of these curves shows that MI from multiple prior eruptive units of Augustine approach and intersect the HSL ± vapor saturation curve given the associated errors. This indicates some of the more felsic fractions of magma were indeed saturated in HSL, and this is consistent with prior observations (Fig. 9) and assumptions. Saturation of Augustine magmas in HSL, with or without vapor, occurred by either direct exsolution in those fractions of evolved melt containing the lowest

H_2O concentrations or, perhaps, by condensation of HSL from the most-H_2O enriched fractions following on the loss of H_2O to CO_2-bearing fluids that could have percolated through the magmas. Sequestration of H_2O from melt into vapor, via gas sparging, as has been described for other CO_2-bearing magmatic systems (Bachmann and Bergantz 2006; Blundy et al. 2010); this process evolves H_2O-enriched melts to comparatively H_2O-poor compositions.

Fluid phase relations with SOHCl-bearing dacitic to rhyolitic melts. We conclude with a brief discussion of the potential consequences of sulfur that was present in Augustine magmas on the exsolution of oxidizing, S-bearing vapor ± HSL. Addressing the role of S is necessary because of prior experimental observations demonstrating that the addition of oxidized S species to silicate melts and coexisting fluids will reduce the maximum observed Cl concentrations of some melts by 25-35 rel% (Botcharnikov et al. 2004; Beermann et al. 2009; Webster et al. 2009; Beermann 2010). This influence of S, on modifying the extent to which Cl dissolves in silicate melts, varies with melt composition and the S contents of the system, and it was observed in runs containing at least 10 wt% SO_2 in the fluid(s).

Regarding f_{O2} and Augustine magmas, Roman et al. (2006), Tappen et al. (2009), Webster et al. (2010), and Larsen et al. (2010) constrained log f_{O2} of NNO+1 to > NNO+2 from coexisting oxide minerals of prehistoric, 1986, and 2006 eruptive units. Zimmer (2009) not only estimated log f_{O2} values of ca. NNO+0.5 suggesting that the basaltic melts were relatively oxidizing, she also measured significant SO_2 in the mafic Augustine MI. Our modeling of closed-system melt evolution requires more than 50% crystallization of the basaltic melt to generate felsic melt compositions. This extent of crystallization would double the SO_2 content of the final, rhyolitic residual melts to values exceeding 1 wt% for magmas that are modeled to be free of sulfides, anhydrite, and fluid phases. This SO_2 abundance,

however, exceeds its solubility in a felsic melt requiring sequestration of some of this sulfur to another phase or phases. We note that anhydrite and iron sulfides have been reported for some eruptive units of Augustine (Johnston 1978; 1979; Tilman 2008), so their presence would also sequester S from melts as they differentiated, but nevertheless, the S contents of evolving Augustine magmas were still potentially significant.

Following on these prior experimental observations, we have revised the data for melt plus OHCl-bearing fluids (Fig. 9) to account for the influence of S in the magmas (Fig. 11A, B, C). The Cl solubilities for S-free melt plus fluid (Fig. 9) have been reduced by both 25 rel% (dotted curve) and 35 (dashed curve) rel% for OHSCl-bearing melts for the maximum 2000-bar *P* and for the lower pressures of each plot (i.e., from 50 to 15 bars). The volatile contents shown in these graphs are much more consistent with the sulfur-reduced Cl solubilities characterizing many of the dacite-rhyolite MI (Fig. 11A) and rhyolite MI (Fig. 11C) at *P* nearer that of the 50-bar and 15-bar HSL- ± vapor-saturation curves, respectively, than the Cl solubility curves for S-free melts (Fig. 9). Comparison of the Cl contents of the rhyodacite-rhyolite MI (Fig. 11B) with the S-enriched, Cl solubility curves indicates saturation in (and buffering of maximum Cl abundances by) HSL ± vapor of a significant number of the MI at *P* approaching 2000 bars. The generation of HSL from shallow, S-bearing magmas of Augustine involved direct exsolution from melt and/or HSL condensation from a preexisting vapor.

This study constrains processes of volatile exsolution and degassing at Augustine for more than 2200 years of its eruptive history. The MI imply entrapment of highly evolved, fluid(s)-saturated rhyolitic melts in phenocrysts at pressures as low and depths as shallow as 70 meters (i.e., for 20 bars *P*). Augustine's crater rims are at approximately 1.2 km elevation, so the most-shallow occurrences of entrapment of fluid(s)-saturated MI took place above sea level

and well within the edifice. Interestingly, seismic hypocenters preceding the 1986 eruption began to ascend from depths of 0.6 km to the crater just nine months before the eruptive phase began (Roman et al. 2006). Similar seismic behavior was also observed before the 1976 (Kienle 1987) and 2006 eruptions (Power and Lalla 2010). These observations are interpreted to signal hydraulic fracturing of overlying rock as magmatic fluid pressure increased (Roman 2006; Power and Lalla 2010). We suggest that these signals may also indicate that the fluid overpressures in Augustine magmas exceeded confining rock strength and indicate separation of magmatic volatile phases from magma at quite shallow-crustal depths. Fluid(s) separation and ascent may have generated some of the recorded seismic behavior and may also open pathways for subsequent magma movement (Roman et al. 2006).

IMPLICATIONS OF THIS INVESTIGATION

Volatile solubility relationships are well established for H_2O-, CO_2-, and H_2S/SO_2-bearing, basaltic to rhyolitic melts, and these relations are essential to interpreting compositions of silicate melt inclusions to understand magmatic degassing processes. The Cl solubility data and model of this study represent a useful advance in our knowledge and application of H_2O-Cl solubility behavior in magmatic systems. These new results are broadly applicable to essentially any geologically relevant melt composition for a wide range of pressures and temperatures, and they allow one to distinguish the presence and role of magmatic hydrosaline liquids with or without chloride-bearing vapors in volcanic as well as mineralizing fluids. These H_2O-Cl solubility relations should prove particularly useful to investigations of CO_2-poor magmas, because it is difficult to determine H_2O-CO_2 solubility relations if the CO_2 contents of melt inclusions are below the limit of detection.

ACKNOWLEDGEMENTS

We appreciate discussions on magmatic volatile behavior with Don Baker. Synthetic apatites were kindly provided by Dan Harlov and Matthias Gottschalk of the GFZ for use as internal standards during our EPMA of Cl. Minerals used in the starting charges of our experiments were provided by the American Museum of Natural History mineral collections. JDW acknowledges and appreciates the efforts and financial support of colleague H. Behrens and those of the University of Hannover, Germany. This assistance was provided while working at the Institut für Mineralogie, Leibniz Universtät Hannover. We appreciate reviews of the manuscript by O. Beermann, an anonymous referee, and Editor T. Mueller. This research was supported by NSF award EAR-0836741 to JDW, by Marie Curie Fellowship IEF_SolVoM #297880 to FV, and DFG funding (project Bo2941-2) for REB.

REFERENCES CITED

Aiuppa, A., Baker, D.R., and Webster, J.D. (2009) Halogens in volcanic systems. Chemical Geology, 263, 1-18.

Alletti, M., Baker, D.R., Scaillet, B., Aiuppa, A., Moretti, R., and Ottolini, L. (2009) Chlorine partitioning between a basaltic melt and H_2O-CO_2 fluids at Mount Etna. Chemical Geology, 263, 37-50.

Baasner, A., Schmidt, B.C., and Webb, S.L. (2013) Compositional dependence of the rheology of halogen (F, Cl) bearing aluminosilicate melts. Chemical Geology, 346, 172-183.

Bachmann, O. and Bergantz, G.W. (2006) Gas percolation in upper-crustal silicic crystal mushes as a mechanism for upward heat advection and rejuvenation of near-solidus magma bodies. Journal of Volcanology and Geothermal Research, 149, 85-102.

Beermann, O. (2010) The solubility of sulfur and chlorine in H_2O-bearing dacites of Krakatau and basalts of Mt. Etna. Unpub. PhD Thesis, 109 p., Hannover.

Beermann, O., Botcharnikov, R.E., Nowak, M., and Holtz, F. (2009) Redox control on S and Cl partitioning between basaltic melts and coexisting fluids: experimental constraints at 1050°C and 200 MPa (abs.). EOS American Geophysical Union, 90(52), V43B-2230.

Bell, A.S. and Simon, A. (2011) Experimental evidence for the alteration of the $Fe^{3+}/\Sigma Fe$ of silicate melt caused by the degassing of chlorine-bearing aqueous volatiles. Geology, 39, 499-502.

Benne, D. and Behrens, H. (2003) Water solubility in haplobasaltic melts. European Journal of Mineralogy, 15, 803–814.

Berndt, J., Liebske, C., Holtz, F., Freise, M., Nowak, M., Ziegenbein, D., Hurkuck, W., and Koepke, J. (2002) A combined rapid-quench and H_2-membrane setup for internally heated pressure vessels: description and application for water solubility in basaltic melts. American Mineralogist, 87, 1717–1726.

Blundy, J., Cashman, K.V., Rust, A., and Witham, F. (2010) A case for CO_2-rich arc magmas. Earth and Planetary Science Letters, 290, 289-301.

Bodnar, R.J., Burnham, C.W., and Sterner, S.M. (1985) Synthetic fluid inclusions in natural quartz. III. Determination of phase equilibrium properties in the system H_2O-NaCl to 1000° C and 1500 bars. Geochimica et Cosmochimica Acta, 49, 1861-1873.

Botcharnikov, R.E., Behrens, H., Holtz, F., Koepke, J., and Sato, H. (2004) Sulfur and chlorine solubility in Mt. Unzen rhyodacite melt at 850°C and 200 MPa. Chemical Geology, 213, 207-225.

Botcharnikov, R.E., Holtz, F., and Behrens, H. (2007) The effect of CO_2 on the solubility of H_2O-Cl fluids in andesitic melt. European Journal of Mineralogy, 19, 61-680.

Bowers, T.S. and Helgeson, H.C. (1983) Calculation of the thermodynamic and geochemical consequences of non-ideal mixing in the system H_2O-CO_2-NaCl on phase relations in geologic systems: Equation of state for H_2O-CO_2-NaCl fluids at high pressures and temperatures. Geochimica et Cosmochimica Acta, 47, 1247-1275.

Burnham CW (1997) Magmas and hydrothermal fluids. In H.L. Barnes, Ed., Geochemistry of Hydrothermal Ore Deposits, 3rd edition, p. 63-123. John Wiley & Sons, New York.

Candela, P.A. and Piccoli, P.M. (1995) Model ore-metal partitioning from melts into vapor and vapor/brine mixtures. In J.F.H. Thompson, Ed., Magmas, Fluids and Ore Deposits, p. 101-127, Mineralogical Society of Canada, 23.

Carroll, M.R. (2005) Chlorine solubility in evolved alkaline magmas. Annals of Geophysics, 48, 619-631.

Carroll, M.R. and Webster, J.D. (1994) Solubilities of sulfur, noble gases, nitrogen, chlorine, and fluorine in magmas. Reviews in Mineralogy, 30, 231-279.

Chevychelov, V.Y. and Suk, N.I. (2003) Influence of the composition of magmatic melt on the solubility of metal chlorides at pressures of 0.1-3.0 kbar. Petrology, 11, 62-74.

Chevychelov, V.Y. and Chevychelova, T.K. (1997) Partitioning of Pb, Zn, W, Mo, Cl, and major elements between aqueous fluid and melt in the systems granodiorite (granite, leucogranite)-H_2O-NaCl-HCl. Neues Jahrbuch für Mineralogie – Abhandlungen, 172, 101-115.

Chevychelov, V.Y., Simakin, A.G., and Bondarenko, G.V. (2003) Mechanism of chlorine dissolution in water-saturated model granodiorite melt: applications of IR spectroscopic methods. Geochemistry International, 41, 4, 395-409.

Chevychelov, V.Y., Botcharnikov, R.E., and Holtz, F. (2008) Experimental study of fluorine and chlorine partitioning between fluid and subalkaline basaltic melt. Doklady Akademii Nauk, 422, 93-97.

Chou, I.-M. (1987) Phase relations in the system NaCl-KCl-H_2O, III: solubilities of halite in vapor-saturated liquids above 445°C and redetermination of phase equilibrium properties in

the system NaCl-H_2O to 1000°C and 1500 bars. Geochimica et Cosmochimica Acta, 51, 1965-1975.

Coombs, M. and Vazquez, J. (2012) Augustine volcano's late Pleistocene rhyolite eruption and its modern-day residuum (abs.). American Geophysical Union Meeting, V43D-2890.

Driesner, T. and Heinrich, C.A. (2007) The system H_2O-NaCl. Part. I: correlation formulae for phase relations in temperature-pressure-composition space from 0 to 1000°C, 0 to 5000 bar, and 0 to 1 X_{NaCl}. Geochimica et Cosmochimica Acta, 71, 4880-4901.

Filiberto, J. and Treiman, A.H. (2009) Martian magmas contained abundant chlorine, but little water. Geology, 37(12), 1087-1090.

Heinrich, W. (2007) Fluid immiscibility in metamorphic rocks. In A. Leibscher and C. Heinrich, Eds., Fluid-Fluid Equilibria in the Crust, p. 389-430, Mineralogical Society of America, 65

Iwasaki, B. and Katsura, T. (1967) The solubility of hydrogen chloride in volcanic rock melts at a total pressure of one atmosphere and at temperatures of 1200° C and 1290° C under anhydrous conditions. Bulletin of the Chemical Society of Japan, 40, 554-561.

Johnston, D.A. (1978) Volatiles, magma mixing, and the mechanism of eruption of Mt. St. Augustine Volcano, Alaska: Seattle, Washington, University of Washington, Unpub. Ph.D. dissertation, 177 p.

Johnston, D.A. (1979) Onset of volcanism at Mt. St. Augustine Volcano, Lower Cook Inlet: U.S. Geological Survey Circular, 804-B, 78–80.

Keinle, J. (1987) Mt. St. Augustine works, but how? Proceedings, Hawaii Symposium on How Volcanoes Work., p. 139.

Kilinc, I.A. and Burnham, C.W. (1972) Partitioning of chloride between a silicate melt and coexisting aqueous phase from 2 to 8 kilobars. Economic Geology, 67, 231-235.

Kotlova, A.G., Ol'shanskii, Y.I., and Tsvetkov, A.I. (1960) Some trends in immiscibility effects in binary silicate and borate systems. Mineralogiya i Geokhimiya. Trudi Instituta Geologii Rudnikh Mestorojdenii AN SSSR, 42, p. 3.

Larsen, J.F., Nye, C.J., Coombs, M.L., Tilman, M., Izbekov, P., and Cameron, C. (2010) Petrology and geochemistry of the 2006 eruption of Augustine Volcano. In J.A. Power, M.L. Coombs, and J.T. Freymueller, Eds., The 2006 Eruption of Augustine Volcano, Alaska, p. 322-383. U.S. Geological Survey Professional Paper 1769.

Liu, Y., Zhang, Y., and Behrens, H. (2005) Solubility of H_2O in rhyolitic melts at low pressures and a new empirical model for mixed H_2O-CO_2 solubility in rhyolitic melts. Journal of Volcanology and Geothermal Research, 143, 219-235.

Lowenstern, J.B. (1994) Chlorine, fluid immiscibility, and degassing in peralkaline magmas from Pantelleria, Italy. American Mineralogist, 79, 353-369.

MacDonald, R., Bailey, D.K., and Sutherland, D.S. (1970) Oversaturated peralkaline glassy trachytes from Kenya. Journal of Petrology, 11, 507-517.

Malinin, S.D., Kravchuk, I.F., and Delbove, F. (1989) Chloride distribution between phases in hydrated and dry chloride-aluminosilicate melt systems as a function of phase composition. Geochemistry International, 26, 32-38.

Metrich, N. and Rutherford, M.J. (1992) Experimental study of chlorine behavior in hydrous silicic melts. Geochimica et Cosmochimica Acta, 56, 607-616.

Moore, G., Vennemann, T., and Carmichael, I.S.E. (1998) An empirical model for the solubility of H_2O in magmas to 3 kilobars. American Mineralogist, 83, 36-42.

Moretti, R., Papale, P., and Ottonello, G. (2003) A model for the saturation of C-O-H-S fluids in silicate melts. Geological Society of London Special Publication, 213, 81-101.

Newman, S. and Lowenstern, J.B. (2002) VOLATILECALC: a silicate melt-H_2O-CO_2 solution model written in Visual Basic for excel. Computers & Geosciences, 28, 597-604.

Pallister, J.S., Thornber, C.R., Cashman, K.V., Clynne, M.A., Lowers, H.A., Mandeville, C.W., Brownfield, I.K., and Meeker, G.P. (2008) Petrology of the 2004-2006 Mount St. Helens lava dome-implications for magmatic plumbing and eruption triggering. In D.R. Sherrod, W.E. Scott, and P.H. Stauffer, Eds., A Volcano Rekindled: The Renewed Eruption of Mount St. Helens, 2004-2006, p. 647-702, U.S. Geological Survey Professional Paper 1750.

Papale, P. (1999) Modeling of the solubility of a two-component H_2O + CO_2 fluid in silicate liquids. American Mineralogist, 84, 477-492.

Power, J.A. and Lalla, D.J. (2010). Seismic observations of Augustine volcano, 1970-2007. In The 2006 eruption of Augustine Volcano, Alaska. In J.A. Power, M.L. Coombs, and J.T. Freymueller, Eds., The 2006 Eruption of Augustine Volcano, Alaska, p. 3-40. U.S. Geological Survey Professional Paper 1769.

Roman, D.C., Cashman, K.V., Gardner, C.A., Wallace, P.J., and Donovan, J.J. (2006) Storage and interaction of compositionally heterogeneous magmas from the 1986 eruption of Mt. St. Augustine Volcano, Alaska. Bulletin of Volcanology, 68, 240-254.

Sandland, T.O., Du, L-S., Stebbins, J.F., and Webster, J.D. (2004) Structure of Cl-containing silicate and aluminosilicate glasses: A ^{35}Cl MAS-NMR study. Geochimica et Cosmochima Acta 68, 5059-5069.

Schettler, G., Gottschalk, M., and Harlov, D.E. (2011) A new semi-micro wet-chemical

method for apatite analysis and its application to the crystal chemistry of fluorapatite-chlorapatite solid solutions. American Mineralogist, 96, 138–152.

Schuessler, J.A., Botcharnikov, R.E., Behrens, H., Misiti, V., and Freda, C. (2008) Oxidation state of iron in hydrous phono-tephritic melts. American Mineralogist, 93, 1493–1504.

Shinohara, H. (1994) Exsolution of immiscible vapor and liquid phases from a crystallizing silicate melt: Implications for chlorine and metal transport. Geochimica et Cosmochimica Acta, 58, 5215-5222.

Shinohara, H. (2009) A missing link between volcanic degassing and experimental studies on chloride partitioning. Chemical Geology, 263, 51-59.

Shinohara, H., Iiyama, J.T., and Matsuo, S. (1989) Partition of chlorine compounds between silicate melt and hydrothermal solutions. Geochimica et Cosmochimica Acta, 53, 2617-2630.

Shmulovich, K.I. and Graham, C.M. (1996) Melting of albite and dehydration of brucite in H_2O-NaCl fluids to 9 kbars and 700-900°C: implications for partial melting and water activities during high pressure metamorphism. Contributions to Mineralogy and Petrology, 124, 370-382.

Signorelli, S. and Carroll, M.R. (2000) Solubility and fluid-melt partitioning of Cl in hydrous phonolitic melts. Geochimica et Cosmochimica Acta, 64, 2851-2862.

Signorelli, S. and Carroll, M.R. (2002) Experimental study of Cl solubility in hydrous alkaline melts: Constraints on the theoretical maximum amount of Cl in trachytic and phonolitic melts. Contributions to Mineralogy and Petrology, 143, 209-218.

Stagno, V., and Dolejs, D. (2008) Experimental study and thermodynamic model for chlorine solubility in polymerized aluminosilicate melts (abs.). Geophysical Research Abstracts, 10 EGU2008-A-03224.

Stebbins, J.F., and Du, L.S. (2002) Chloride ion sites in silicate and aluminosilicate glasses: A preliminary study by 35Cl solid-state NMR. American Mineralogist 87, 359-363.

Stelling J., Botcharnikov, R.E., Beermann, O., and Nowak, M. (2008) Solubility of H_2O- and chlorine-bearing fluids in basaltic melt of Mount Etna at T=1050-1250°C and P=200 MPa. Chemical Geology, 256, 102-110.

Symonds, R.B., Rose, W.I., Gerlach, T.M., Briggs, P.H., and Harmon, R.S. (1990) Evaluation of gases, condensates, and SO_2 emissions from Augustine volcano, Alaska – the degassing of a Cl-rich volcanic system: Bulletin of Volcanology, 52, 355-374.

Tappen, C., Webster, J.D., Roderick, D., Mandeville, C. W. (2009) Petrology and geochemistry of ca. 2100 -1000 a.B.P. magmas of Augustine volcano, Alaska. Journal of Volcanology and Geothermal Research, 183, 42-62.

Tilman, M.R. (2008) An investigation of symplectite-rimmed olivine and magmatic processes during the 2006 eruption of Augustine Volcano, Alaska: University of Alaska, Fairbanks, unpub. M.S. thesis, 166 p.

Webb, S.L., Murton, B.J., Wheeler, A.J. (2014) Rheology and the Fe^{3+}-chlorine reaction in basaltic melts. Chemical Geology, 366, 24-41.

Webster, J.D. (1992a) Fluid-melt interactions involving Cl-rich granites: Experimental study from 2 to 8 kbar. Geochimica et Cosmochimica Acta 56, 679-687.

Webster, J.D. (1992b) Fluid-melt interactions in Cl-rich granitic systems: Effects of melt composition at 2 kbar and 800° C. Geochimica et Cosmochimica Acta, 56, 659-678.

Webster, J.D. (2004) The exsolution of magmatic hydrosaline melts. Chemical Geology, 210, 33-48.

Webster, J.D. (2013) Fluid(s)/melt partitioning of COHSCl volatiles and associated controls on volcanic degassing (abs.). EOS American Geophysical Union, V23E-05.

Webster, J.D. and DeVivo, B. (2002) Experimental and modeled solubilities of chlorine in aluminosilicate melts, consequences of magma evolution, and implications for exsolution of hydrous chloride melt at Mt. Somma-Vesuvius. American Mineralogist, 87, 1046-1061.

Webster, J.D. and Rebbert C.R. (1998) Experimental investigation of H_2O and Cl solubilities in F-enriched silicate liquids: implications for volatile saturation of topaz rhyolite magmas. Contributions to Mineralogy and Petrology, 132, 198-207.

Webster, J.D. and Mandeville, C.W. (2007) Fluid immiscibility in volcanic systems. In A. Leibscher, C. Heinrich, Eds., Fluid-Fluid Equilibria in the Crust, p. 313-362, Reviews in Mineralogy and Geochemistry Volume 65.

Webster, J.D., DeVivo, B. and Tappen, C. (2003) Volatiles, magmatic degassing and eruptions of Mt. Somma-Vesuvius: constraints from silicate melt inclusions, solubility experiments and modeling. In B. De Vivo and R.J. Bodnar, Eds., Melt Inclusions in Volcanic Systems: Methods, Applications and Problems, p. 207-226, Developments in Volcanology 5. Elsevier, Amsterdam.

Webster, J.D., Kinzler, R.J., and Mathez, E.A. (1999) Chloride and water solubility in basalt and andesite liquids and implications for magmatic degassing. Geochimica et Cosmochimica Acta, 63, 729-738.

Webster, J.D., Sintoni, M.F., and De Vivo, B. (2009) The partitioning behavior of Cl and S in aqueous fluid- and saline-liquid saturated phonolitic and trachytic melts at 200 MPa. Chemical Geology, 263, 19-36.

Webster, J.D., Mandeville, C.W., Goldoff, B., Coombs, M.L., Tappen, C. (2010) Augustine volcano, Alaska: the influence of volatile components in magmas erupted AD 2006 to 2100 years before present. In J.A. Power, M.L. Coombs, and J.T. Freymueller, Eds., The 2006 Eruption of Augustine Volcano, Alaska, p. 383-423. U.S. Geological Survey Professional Paper 1769.

Webster, J.D., Goldoff, B.A., Sintoni, M.F., Shimizu, N., and De Vivo, B. (in review) C-O-H-S-Cl-F volatile solubilities, partitioning, and mixing in phonolitic-trachytic melts and aqueous-carbonic vapor ± saline liquid at 200 MPa. In review at the Journal of Petrology.

Witham, R., Blundy, J., Kohn, S.C., Lesne, P., Dixon, J., Chrakov, S.V., and Botcharnikov, R. (2012) SolEx: A model for mixed COHSCl-volatile solubilities and exsolved gas composition in basalt. Computers & Geosciences, 45, 87-97.

Zajacz, Z., Candela, P.A., Piccoli, P.M., and Sanchez-Valle, C. (2012) The partitioning of sulfur and chlorine between andesitic melts and magmatic volatiles and the exchange coefficients of major cations. Geochimica et Cosmochimica Acta, 89, 81-101.

Zimmer, M. M. (2009). Water in Aleutian magmas: Its origin in the subduction zone and its effects on magma evolution, Unpub. PhD thesis, Boston University, Boston, MA, 448 pp.

Figure Captions

1) Schematic curves distinguishing single-fluid condition (faint solid curve) and one- or two-fluid conditions (faint to bold dashed lines) as a function of the H_2O and Cl contents of a coexisting aluminosilicate melt. The curve linking points [1] and [2] bears on Cl partitioning

between a single fluid and the melt (if corresponding Cl contents of fluids are known), and at point [1] H_2O solubility and at point [2] Cl solubility can be extracted for the relevant pressure, temperature, and melt composition. For the one- to two-fluid conditions, the melt compositions at point [3] and along faint dashed line from point [3] up to but not including point [4] bear on Cl partitioning between a single fluid and the melt. These vapor-saturated melt compositions also provide H_2O solubility because of strongly non-ideal volatile behavior. At point [4], along bold dashed line to point [5], and at point [2], Cl solubility can be extracted because the melt is saturated with a Cl-enriched hydrosaline liquid with or without an aqueous vapor.

2) Plot expressing the accuracy of the electron probe microanalysis (EPMA) measurements of Cl in the run-product glasses of this study. The plot compares Cl concentrations of obsidian, NaCl, KCl, scapolite, and several apatites determined by EPMA versus measured (wet chemistry) or theoretical Cl concentrations. Coefficient of fit (R^2 = 0.9998); see text for discussion. One-sigma precision values are less than symbol size.

3) Plot showing the influence of temperature on the solubility of Cl in experimental melts saturated in hydrosaline liquid ± vapor (open circles represent rhyolitic melts with molar N/NK = $[Na_2O/(Na_2O+K_2O)] > 0.55$, and filled circles show rhyolitic melts with molar N/NK] < 0.55 at 2000 bars; the triangles designate phonolitic melts at 5000 bars). Chlorine solubility increases with temperature. Curves are fits to data; representative one-sigma imprecision shown with the cross. See text for discussion.

4) Plot showing the influence of pressure on the molar solubility of Cl (i.e., moles of Cl in 100 grams of silicate melt) normalized to equivalent moles of Ca plus Mg in topaz rhyolitic (circles) melts at 930-1045°C, latitic (squares) melts at 1033-1075°C, phonolitic (triangles)

melts at 1166-1250°C, and basaltic (crosses) melts at 1193-1250°C. Chlorine solubility in hydrosaline liquid- ± vapor-saturated melts decreases with reduced pressure. This relationship is stronger with rhyolitic and phonolitic melts, and these melts show greatest effect at $P \leq 2000$ bars. The pressure effect is weaker with latitic and basalt melts. The topaz rhyolite data include an additional datum for the solubility at 703° corrected to 1000° (large circle) using relationships shown in Figure 3. The phonolitic data also include two additional data for normalized Cl solubilities at lower temperatures of 1000 and 1050°C. Both data lie below the solubility curve for 1166-1250°C because of the influence of temperature on Cl dissolution. Representative one-sigma imprecision shown with the cross.

5) Plot showing inverse correlation of the molar Cl solubility (i.e., moles of Cl in 100 grams of silicate melt) in all 121 hydrosaline liquid- ± vapor-saturated melts of this study and the 41 fluid(s)-saturated melts of Webster and De Vivo (2002) versus the moles of Si in 100 grams of melt.

6) Plot of the molar Cl solubility (i.e., moles of Cl in 100 grams of silicate melt) in hydrosaline liquid- ± vapor-saturated aluminosilicate melts as a function of composition. Chlorine solubility increases with the moles of Al, Ca, Mg, and Na and decreases with the moles of Si in rhyolitic to basaltic melts at 1000-1100°C through the pressure range of ca. 1 to 5000 bars.

7) (A) Plot comparing measured Cl concentrations of 159 CO_2-free, hydrosaline liquid- ± vapor-saturated aluminosilicate melts of this study and Webster and De Vivo (2002) versus Cl concentrations of melts calculated with expanded Cl-solubility model of this study (as triangles) and data of the 4 runs containing 8 - 21 wt% CO_2 in the integrated hydrosaline liquid and vapor distinguished (circles). Model applies to rhyolitic to basaltic melts at 700-1250°C and ca. 1 to 7000 bars. Carbon dioxide-enriched fluids have no detectable influence on Cl

solubility in silicate melts, within precision. Solid curve fit to all data has correlation of fit (R^2) of 0.98; dotted lines show 10 rel% error and dashed lines show 20 rel% error about the solid curve. See text for discussion. (B) Plot comparing measured versus modeled Cl concentrations of 163 melts of these experiments and Webster and De Vivo (2002) (fine diamonds) with those of prior experimental studies of Beermann (2010; diamonds), Signorelli and Carroll (2000; square), Metrich and Rutherford (1992; open circle), Chevychelov et al. (2003; open crosses), Botcharnikov et al. (2004; upward-directed triangle), Botcharnikov et al. (2007; down-pointing triangle), Chevychelov et al. (2008; filled circle).

8) Schematic plots comparing (A) volatile-solubility behavior for H_2O and Cl in dacitic melts and (B) relevant sub-solvus and near-solvus phase relations in the melt-free system NaCl-H_2O based on phase equilibria of Bodnar et al. (1985). With increasing Cl in the system in (A), melt coexists with vapor at near-solvus point [3], with vapor plus hydrosaline (HSL) liquid (subsolvus conditions) at point(s) [4], and with HSL only at near-solvus point [2] at 1500 bars and 900°C (solid and dashed bold lines). These conditions correspond to line [3] to [5] in plot (B). Strongly non-ideal mixing of volatiles in fluid(s) at these sub- and near-solvus conditions (in B) buffers the H_2O and Cl concentrations of coexisting melt. Chlorine concentrations in this Mt. St. Helens dacite (Pallister et al. 2008) composition were calculated with expanded Cl solubility model of this study and maximum H_2O contents calculated with solubility model of Moore et al. (1998). Faint solid curve (from points [1] to [2] in [A]) represents schematic H_2O and Cl concentrations of dacitic melt saturated in vapor only or hydrosaline liquid only at arbitrarily chosen near-solvus fluid conditions of 2000 bars and 900°C. These conditions correspond to line [1] to [2] in plot (B).

9) Plots comparing Cl and apparent H_2O contents in silicate melt inclusions (MI) from Augustine volcano, Alaska, with modeled H_2O-Cl solubility curves expressing the stability of OHCCl-bearing vapor-only, vapor plus hydrosaline liquid, or hydrosaline liquid-only conditions. The dashed, double-lined curve represents the locus of vapor plus hydrosaline stability points as pressure decreases from 2000 bars in each plot. Plot (A) compares H_2O and Cl concentrations in basaltic to basaltic-andesite MI with curves for basaltic melts at 1100°C and 2000 bars (fine lines) and 90 bars (bold lines). Plot (B) compares H_2O and Cl contents of dacitic to rhyodacitic MI with curves for dacitic melts at 1000°C and 2000 bars (faint solid lines) and rhyodacitic melts at 900°C and 1125 bars (dot-dash lines), 500 bars (bold dashed lines), and 50 bars (bold solid lines). In (C), volatile concentrations of rhyodacitic to rhyolitic MI indicate that most were trapped at pressures < 2000 bars from vapor-saturated magma; whereas 9 MI represent entrapment of hydrosaline- and vapor-saturated magmas at pressures of 25 to 2000 bars. In (D) for rhyolitic melts, most MI reflect melt entrapment of vapor-saturated magma at pressures between 15 and 2000 bars, but several MI are consistent with their entrapment at pressures as low as 15 bars, from felsic magma that was saturated in hydrosaline liquid and vapor. Open triangles pointing left represent MI of 1000 ybp prehistoric unit, open triangles pointing down are MI of 1010 ybp prehistoric unit, filled triangles pointing lower-left represent MI of 1700 ybp prehistoric unit, open triangles pointing up represent MI of 1400 ybp prehistoric unit, and filled triangles pointing lower-right represent MI of 2100 ybp prehistoric unit (Tappen et al. 2009). Filled triangles pointing down (Webster 2013) and filled triangles pointing up (Zimmer 2009) represent MI of ca. 26,000-year old basalt. Squares and crosses designate MI from 2006 eruptive units (Webster et al. 2010), and diamonds represent MI from 1986 eruptive materials (Roman et al. 2006; Webster 2013).

10) Plots expressing how (A) the Cl concentrations of silicate melt inclusions (MI) vary as a function of magma evolution at Augustine volcano, Alaska (i.e., expressed as the Larsen melt differentiation index), and (B) the calculated solubility of Cl in melt compares with measured Cl concentrations for these MI compositions. Graph (A) applies compositions of MI from ca. 26,000-year old basaltic rocks to represent that of parent or source magma. The arrow expresses the increase in Cl concentrations of fractions of residual melt as fluid-absent basaltic magma fractionally crystallizes to rhyolitic melt. The comparatively lower concentrations of Cl in MI indicate the sequestration of Cl from evolving melt by vapor and/or hydrosaline liquid; fluid or fluids exsolved at dacitic stage of magma evolution. The arrow in graph (B) expresses how the solubility of Cl decreases with the progressive magma evolution represented in (A). The dashed curve is a 1:1 correspondence line that expresses the maximum, predicted Cl solubilities for the rhyolitic MI compositions because these MI compositions are saturated in hydrosaline liquid ± vapor at the pressures and temperatures of felsic Augustine melts. The measured (actual) Cl concentrations of the most Cl-enriched fractions of residual melt are limited or buffered by the presence of hydrosaline liquid during magma evolution.
11) Plots comparing Cl and apparent H_2O contents in silicate melt inclusions (MI) from Augustine volcano, Alaska, with modeled H_2O-Cl solubility curves expressing the stability of OHSCl-bearing vapor-only, vapor plus hydrosaline liquid, or hydrosaline liquid-only conditions. The stability curves express Cl solubilities that have been reduced by 25 rel% (dashed) and 35 rel% (dotted) – relative to values predicted by the model of this study - for melts containing oxidized sulfur because of the observed experimental influence of S on Cl dissolution (Botcharnikov et al. 2004; Beermann et al. 2009; Webster et al. 2009; Beerman 2010). The dashed, double-lined curve represents the locus of vapor plus hydrosaline stability

points as pressure decreases from 2000 bars in each plot. Comparison of the plotted Cl concentrations of melt inclusions in graphs (A) for dacitic-rhyolitic, (B) for rhyodacitic-rhyolitic, and (C) rhyolitic eruptive units with fluid-stability, volatile-solubility curves suggests that numerous rhyodacitic and rhyolitic MI reflect saturation in hydrosaline liquid.

APPENDIX

Computation methods for expanded empirical Cl solubility model

This model follows on the 2000-bar method of Webster and De Vivo (2002) modified for subtle issues of composition and accounting for changes in pressure and temperature. At ca. 1 to 7000 bars, 700° to 1250°C, the quantity of Cl that dissolves in aluminosilicate melts of rhyolitic to basaltic composition is described by (i.e., all [X] quantities are in moles per 100 grams of melt and are calculated as the [wt% component/molecular or atomic weight of the component]):

A) The 2000-bar molar solubility of Cl (moles Cl in 100 grams of melt) not accounting for pressure or temperature =

[[Cl]@2000bar] =

((((0.00566)x[Al]) + ((0.0105)x[K]) + ((0.04)x[Na]) + ((0.143)x[Fe]) + ((0.24)x[Ca]) + ((0.25)x[Mg]) + ((0.0636)x[F]))

- ([Ti]x(1)) ***IF*** [Si] < 0.975
{FOR Ti-BEARING, MAFIC MELTS}

- ([P]x(1.3)) ***IF*** [P] < 0.08 ***AND*** [Si] < 1
{FOR P-BEARING, MAFIC MELTS}

- ((0.02)x([Ca]+(2x[Na])+(2x[K])))/(2x[Al]) ***IF***
(2x[Al])/([Ca]+(2x[Na])+(2x[K]))) < 0.7 ***AND***
([Na])/([Na])+([K]))) < 0.32
{FOR RELATIVELY POTASSIC, ALKALINE MELTS}

+ ([P]x(0.07)) ***IF*** [Si] > 1
{FOR P-BEARING, INTERMEDIATE AND FELSIC MELTS}

+ (([Al]-([Na]+[K]+[Ca]+[Li]))x(0.15)) ***IF*** [Si] > 1.1 ***AND*** ([Al]/([Ca]+[Na]+[K]+[Li])) > 1.19
{FOR ALUMINOUS FELSIC MELTS}

+ ((([Na]+[K]+[Ca]+[Li])-[Al])x(0.0055)) ***IF*** [Si] > 1.0 ***AND*** (([Ca]+[Na]+[K]+[Li])/[Al]) > 1.1
{FOR ALKALINE, INTERMEDIATE AND FELSIC MELTS}

+ (([Al]+[Ca]+[Mg])/([Na]+[K]+[Li])x(0.0015)) ***IF*** (([Al]+[Ca]+[Mg])/([Na]+[K]+[Li])) > 10 *{FOR Al-, Ca-, AND Mg-ENRICHED MAFIC MELTS}*

B) The molar solubility of Cl in 100 grams of melt at all pressures (in bars) and temperatures (in degrees Celsius) =

[[Cl]@P&T] =

[[Cl]@2000bar]

+ (([[Cl]@2000bar] x ((pressure) – (1999)) x (0.00011)) ***IF*** pressure > 2100

+ (([[Cl]@2000bar] x ((pressure) – (1999)) x (0.0001)) ***IF*** pressure < 2000

+ **((**[[Cl]@2000bar] x ((temperature) – (1050)) x (0.0008)) ***IF*** temperature > 1050 ***AND*** [Si] > 0.93

C) The wt% of Cl in 100 grams of melt (at all pressures and temperatures) =

([[Cl]@P&T] x (35.453))

TABLE 1. Starting materials and experimental run conditions for chlorine solubility experiments

Experiment Number[a]	P (bars)	T (°C)	Starting Material Bulk Composition	Chlorides Added to Starting Charge	Hydrogen Pressure Applied[b]	Run Duration (hrs).	Run-Product Phases[c]
1atm-96-3A	ca. 1[d]	1160	andesite	NaCl, KCl	≈ 0.69 bars	184	s, g, c, p, FeTi
1atm-96-3B	ca. 1[d]	1160	andesite	NaCl, KCl	≈ 0.69 bars	184	s, g, p, FeTi
1atm-96-3C	ca. 1[d]	1160	latite	NaCl, KCl	≈ 0.69 bars	184	s, g
1atm-97-2A	ca. 1[d]	1045	topaz rhyolite	NaCl, KCl	≈ 0.69 bars	136	s, g
1atm-95-1A	ca. 1[d]	1055	granite	NaCl, KCl	≈ 0.69 bars	157	s, g
1atm-95-1C	ca. 1[d]	1055	granite	NaCl, KCl	≈ 0.69 bars	157	s, g
1atm-95-3H	ca. 1[d]	1055	granite	NaCl, KCl	≈ 0.69 bars	140	s, g
1atm-95-4	ca. 1[c]	1050	granite	NaCl, KCl	≈ 0.69 bars	279	s, g
1atm-96-2B	ca. 1[d]	1075	haplogranite	NaCl, KCl	≈ 0.69 bars	182	s, g
1atm-96-2C	ca. 1[d]	1075	topaz rhyolite	NaCl, KCl	≈ 0.69 bars	182	s, g, p, FeTi
1atm-96-2A	265	1075	latite	NaCl, KCl	≈ 0.69 bars	182	s, g, p, FeTi
CS-13-18A	265	700	granite	NaCl, KCl	≈ 0.69 bars	*455*	s,g,p,q,ft
CS-13-18B	483	700	granite	NaCl, KCl	≈ 0.69 bars	*455*	s,g,p,q,ft
1-12-16A	483	1135	andesite	$PtCl_2$	≈ 0.69 bars	290	s, g, p, FeTi
1-12-16B	483	1135	phonotephrite	$PtCl_2$	≈ 0.69 bars	290	s, g
1-12-16C	500	1135	dacite	$PtCl_2$	≈ 0.69 bars	290	s, g
1-02-12A	500	1001	phonolite	NaCl, KCl	≈ 0.69 bars	168	s, g
1-02-19A	500	1000	phonolite	NaCl, KCl	≈ 0.69 bars	115	s, g, FeTi
1-02-12C	500	1001	phonolite, H_2O	NaCl, KCl	≈ 0.69 bars	168	s, g, FeTi
1-99-3A	500	1122	phonotephrite	NaCl, KCl, $FeCl_2{\cdot}4H_2O$	≈ 0.69 bars	98	s, g
1-95-10D	500	910	topaz rhyolite, H_2O	NaCl, KCl	≈ 0.69 bars	268	s, g

1-95-10G	500	930	topaz rhyolite	NaCl, KCl	≈ 0.69 bars	257	s, g
1-09-14C	500	909	rhyodacite, H_2O, H_3PO_4, NaF, apatite	$CaCl_2 \cdot 2H_2O$	≈ 0.69 bars	386	s, g, a, p, c, FeTi
1-09-15B	500	900	rhyodacite, H_2O, H_3PO_4, NaF, apatite	$CaCl_2 \cdot 2H_2O$, NaCl, KCl, HCl	≈ 0.69 bars	525	s, g, a, p, c, FeTi
1-09-15C	500	900	rhyodacite, H_2O, H_3PO_4, NaF, apatite	$CaCl_2 \cdot 2H_2O$, NaCl, KCl, HCl	≈ 0.69 bars	525	s, g, a, p, c, FeTi
1-95-9E	500	931	granite, H_2O	NaCl, KCl	≈ 0.69 bars	*142*	s, g
1-95-9A	500	931	granite	NaCl, KCl	≈ 0.69 bars	*142*	s, g
1-95-9B	500	931	granite	NaCl, KCl	≈ 0.69 bars	*142*	s, g
1-95-9C	500	931	granite, H_2O	NaCl, KCl	≈ 0.69 bars	*142*	s, g
1-95-9G	507	931	granite	NaCl, KCl	≈ 0.69 bars	*142*	s, g
1-09-16A	507	1122	rhyodacite, H_2O	$CaCl_2 \cdot 2H_2O$	≈ 0.69 bars	168	s, g
1-09-16D	510	1122	rhyodacite	NaCl, $CaCl_2 \cdot 2H_2O$	≈ 0.69 bars	168	s, g
1-94-22D	510	1065	haplogranite	NaCl, KCl	≈ 0.69 bars	*499*	s, g
1-94-22A	510	1065	haplogranite	NaCl, KCl	≈ 0.69 bars	*499*	s, g
1-94-22C	510	1065	haplogranite	NaCl, KCl	≈ 0.69 bars	*499*	s, g
1-94-22B	510	1065	haplogranite, H_2O	NaCl, KCl	≈ 0.69 bars	*499*	s, g
1-94-22E	550	1065	haplogranite	NaCl, KCl	≈ 0.69 bars	*499*	s, g
1-94-23D	550	860	haplogranite	NaCl, KCl	≈ 0.69 bars	*452*	s, g, q
1-94-23F	550	860	haplogranite	NaCl, KCl	≈ 0.69 bars	*452*	s, g, q
1-94-23H	550	860	haplogranite	NaCl, KCl	≈ 0.69 bars	*452*	s, g, q
1-94-23C	550	860	haplogranite	NaCl, KCl	≈ 0.69 bars	*452*	s, g, q
1-94-23B	1000	860	haplogranite	NaCl, KCl	≈ 0.69 bars	*452*	s, g
2012-H5-6	1000	1250	basalt	$PtCl_4$	≈ 0.69 bars	72	s, g

2012-H5-4	1000	1250	andesite	$PtCl_4$	≈ 0.69 bars	72	s, g
2012-H5-2	1000	1250	phonolite	$PtCl_4$	≈ 0.69 bars	72	s, g
2012-H5-5	1000	1250	rhyolite	$PtCl_4$, NaCl, KCl	≈ 0.69 bars	72	s, g
2012-H5-1	1000	1250	phonotephrite	$PtCl_4$	≈ 0.69 bars	72	s, g
2012-H5-3	1000	1250	dacite	$PtCl_4$	≈ 0.69 bars	72	s, g
1-95-12E	1000	1060	granite	NaCl, KCl	≈ 0.69 bars	308	s, g
1-95-12B	1000	1060	granite	NaCl, KCl	≈ 0.69 bars	308	s, g
1-97-3A	1000	965	haplogranite	NaCl, KCl	≈ 0.69 bars	258	s, g
1-97-3C	1450	965	haplogranite	NaCl, KCl	≈ 0.69 bars	258	s, g
1-99-1B	1500	985	andesite, H_2O	$FeCl_2{\cdot}4H_2O$	29 bars	213	s, g, p, c, FeTi
1-00-18A	1500	1160	anorthite-diopside mix	$CaCl_2$, $MgCl_2$	≈ 0.69 bars	142	s, g
1-00-18B	1500	1160	anorthite-diopside mix	$CaCl_2$, $MgCl_2$	≈ 0.69 bars	142	s, g
1-00-23A	1500	1158	anorthite-diopside mix	$PtCl_2$	≈ 0.69 bars	165	s, g
1-00-23B	1500	1158	anorthite-diopside mix	$PtCl_2$	≈ 0.69 bars	165	s, g
1-00-23C	1500	1158	anorthite-diopside mix	$PtCl_2$	≈ 0.69 bars	165	s, g
1-00-23D	1500	1158	anorthite-diopside mix	$PtCl_2$	≈ 0.69 bars	165	s, g
1-00-23E	1500	1158	anorthite-diopside mix	$PtCl_2$	≈ 0.69 bars	165	s, g
1-00-28A	1500	1100	anorthite-diopside mix	$PtCl_2$	≈ 0.69 bars	138	s, g
1-00-28B	1500	1100	anorthite-diopside mix	$PtCl_2$	≈ 0.69 bars	138	s, g
1-00-28C	1500	1100	anorthite-diopside mix	$PtCl_2$	≈ 0.69 bars	138	s, g
1-00-28D	1500	1100	anorthite-diopside mix	$PtCl_2$	≈ 0.69 bars	138	s, g
1-00-28F	1500	1100	anorthite-diopside mix	$PtCl_2$	≈ 0.69 bars	138	s g
1-01-35B	1500	1050	anorthite-diopside mix	$PtCl_2$	≈ 0.69 bars	140	s, g
1-01-35C	1980	1050	anorthite-diopside mix	$PtCl_2$	≈ 0.69 bars	140	s, g

1-07-13A	1980	990	rhyodacite, H_2O, apatite, Fe_3O_4	NaCl, KCl	≈ 0.69 bars	648	s, g, a
1-07-13B	2000	990	rhyodacite, H_2O, apatite, Fe_3O_4	NaCl, KCl	≈ 0.69 bars	648	s, g, a
1-00-32B	2000	1151	anorthite-diopside mix	$PtCl_2$	≈ 0.69 bars	211	s, g
1-00-32C	2000	1151	anorthite-diopside mix	$PtCl_2$	≈ 0.69 bars	211	s, g
1-02-11A	2000	997	phonolite	NaCl, KCl	≈ 0.69 bars	190	s, g, a, p, c, FeTi
1-07-05[e]	2000	903	phonolite, H_2O, CO_2	NaCl, KCl, $C_2H_2O_4{\cdot}2H_2O$	≈ 0.69 bars	*245*	s, g
1-07-06[f]	2000	901	phonolite, H_2O, CO_2	NaCl, KCl, $C_2H_2O_4{\cdot}2H_2O$	≈ 0.69 bars	*263*	s, g
1-94-17A	2000	972	F-rich topaz rhyolite	NaCl, KCl	≈ 0.69 bars	*163*	s, g
1-94-17B	2000	972	topaz rhyolite	NaCl, KCl	≈ 0.69 bars	*163*	s, g
1-10-07A[g]	2000	900	haplogranite, H_2O, CO_2, S	NaCl, KCl, $C_2H_2O_4{\cdot}2H_2O$	≈ 0.69 bars	*602*	s, g
1-96-13E[h]	2000	950	haplogranite, H_2O, CO_2	NaCl, KCl, $C_2H_2O_4{\cdot}2H_2O$	≈ 0.69 bars	*195*	s, g
1-96-13D	2010	950	haplogranite	NaCl, KCl	≈ 0.69 bars	*195*	s, g
1-99-15	2020	1100	basalt, H_2O, H_3PO_4, apatite	NaCl, KCl, $FeCl_2{\cdot}4H_2O$, $CaCl_2{\cdot}2H_2O$	36 bars	136	s, g, a, o, FeTi
1-94-1D	2030	703	topaz rhyolite	NaCl, KCl	≈ 0.69 bars	187	s, g
1-03-09B	2040	958	phonolite	$CaCl_2{\cdot}2H_2O$	≈ 0.69 bars	240	s, g
1-99-12	2000	1104	basalt, H_2O, H_3PO_4, apatite	NaCl, KCl, $FeCl_2{\cdot}4H_2O$	38 bars	117	s, g, a, o, FeTi
1-00-19B	3010	1075	basalt, apatite, Fe_3O_4	$FeCl_2{\cdot}4H_2O$, $CaCl_2{\cdot}2H_2O$	15 bars	138	s, g, a, c, o, FeTi
1-96-1B	3010	1015	haplogranite	NaCl, KCl	≈ 0.69 bars	132	s, g
1-96-1E	3010	1015	haplogranite, H_2O	NaCl, KCl	≈ 0.69 bars	132	s, g
1-96-1D	3010	1015	haplogranite	NaCl, KCl	≈ 0.69 bars	132	s, g
1-96-1F	3010	1015	haplogranite, H_2O	NaCl, KCl	≈ 0.69 bars	132	s, g
1-96-1A	3010	1015	haplogranite, H_2O	NaCl, KCl	≈ 0.69 bars	132	s, g
1-96-1C	3000	1015	haplogranite	NaCl, KCl	≈ 0.69 bars	132	s, g

2012-H2-1	3000	1250	phonolite	$PtCl_4$	≈ 0.69 bars	72	s, g
2012-H2-2	3000	1250	andesite	$PtCl_4$	≈ 0.69 bars	72	s, g
2012-H2-3	3000	1250	basalt	$PtCl_4$	≈ 0.69 bars	72	s, g
2012-H2-4	3000	1250	phonotephrite	$PtCl_4$	≈ 0.69 bars	72	s, g
2012-H2-5	3000	1250	dacite	$PtCl_4$	≈ 0.69 bars	72	s, g
2012-H2-6	3940	1250	rhyolite	$PtCl_4$, NaCl, KCl	≈ 0.69 bars	72	s, g
1-95-8B	4000	843	haplogranite	NaCl, KCl	≈ 0.69 bars	305	s, g
1-96-5A	4000	950	haplogranite	NaCl, KCl	≈ 0.69 bars	*286*	s, g
1-96-5E	4000	950	albite-quartz	NaCl	≈ 0.69 bars	*286*	s, g
1-96-5F	4070	950	orthoclase-quartz	KCl	≈ 0.69 bars	*286*	s, g
1-95-11A	4070	1047	haplogranite	NaCl, KCl	≈ 0.69 bars	*239*	s, g
1-95-11E2	4070	1047	haplogranite, H_2O	NaCl, KCl	≈ 0.69 bars	*239*	s, g
1-95-11E	4070	1047	haplogranite, H_2O	NaCl, KCl	≈ 0.69 bars	*239*	s, g
1-95-11B2	4470	1047	haplogranite, H_2O	NaCl, KCl	≈ 0.69 bars	*239*	s, g
1-97-10A	4470	1058	haplogranite	NaCl, KCl	≈ 0.69 bars	121	s, g
1-97-10B	4470	1058	haplogranite	NaCl, KCl	≈ 0.69 bars	121	s, g
1-97-10C	5000	1058	latite	NaCl, KCl	≈ 0.69 bars	121	s, g
2012-H1-1	5000	1250	basalt	$PtCl_4$	≈ 0.69 bars	72	s, g
2012-H1-2	5000	1250	andesite	$PtCl_4$	≈ 0.69 bars	72	s, g
2012-H1-3	5000	1250	phonolite	$PtCl_4$	≈ 0.69 bars	72	s, g
2012-H1-5	5000	1250	phonotephrite	$PtCl_4$	≈ 0.69 bars	72	s, g
2012-H1-4	5000	1250	rhyolite	$PtCl_4$, NaCl, KCl	≈ 0.69 bars	72	s, g
2012-H3-1	5000	1050	phonolite	$PtCl_4$	≈ 0.69 bars	120	s, g
2012-H3-2	5000	1050	dacite	$PtCl_4$	≈ 0.69 bars	120	s, g

2012-H3-3	5000	1050	rhyolite	$PtCl_4$	≈ 0.69 bars	120	s, g
2012-H3-4	7000	1050	rhyolite	NaCl, KCl	≈ 0.69 bars	120	s, g
2012-H4-2	7000	1250	phonotephrite	$PtCl_4$	≈ 0.69 bars	120	s, g
2012-H4-3	7000	1250	dacite	$PtCl_4$	≈ 0.69 bars	120	s, g
2012-H4-4	7000	1250	phonolite	$PtCl_4$	≈ 0.69 bars	120	s, g
2012-H4-5	7000	1250	andesite	$PtCl_4$	≈ 0.69 bars	120	s, g
2012-H4-6	7000	1250	rhyolite	$PtCl_4$, NaCl, KCl	≈ 0.69 bars	120	s, g

[a]Runs with 2012-Hx-x designation conducted at the University of Hannover, Germany; all other runs conducted at American Museum of Natural History.

[b]H_2 pressure applied during run. The ca. 0.69 bars value is ambient IHPV pressure; higher pressures were applied by Shaw membrane.

[c]Phases in run products: s=salts, g= vesicular glass, q=quartz, p=plagioclase, c=clinopyroxene, o=orthopyroxene, FeTi=iron titanium oxides.

[d]Runs at ca. 1-bar pressure conducted at ambient pressure in sealed precious metal capsules that may have contained internal pressures marginally 1 atm.

[e]Hydrosaline liquid composition computed (with mass balance) to contain ca. 16 wt% CO_2, 22 wt% Cl, 41 wt% H_2O, and 21 wt% cations at run conditions.

[f]Hydrosaline liquid composition computed (with mass balance) to contain ca. 8 wt% CO_2, 16 wt% Cl, 61 wt% H_2O, and 15 wt% cations at run conditions

[g]Hydrosaline liquid composition computed (with mass balance) to contain ca. 2 wt% S, 17 wt% Cl, 21 wt% CO_2, 45 wt% H_2O, and 15 wt% cation at run conditions

[h]Hydrosaline liquid composition computed (with mass balance) to contain ca. 8 wt% H_2O, 21 wt% CO_2, 36 wt% Cl, 35 wt% cations at run conditions.

TABLE 2. Compositions (in wt%) of run-product glasses of Cl solubility experiments and modeled Cl solubilities

Experiment Number	SiO_2	TiO_2	Al_2O_3	MnO	MgO	FeO[a]	CaO	Na_2O	K_2O	P_2O_5	F	Cl	SO_2	Total	Molar A/CNK[b]	Molar N/NK[c]	Modeled Cl Solubility[d]
1atm-96-3A	55.14	1.02	17.11	0.12	4.57	6.96	8.22	4.10	1.51	0.15	0.02	1.42	nd[e]	100.34	0.73	0.80	1.90
1atm-96-3B	55.92	1.01	17.35	0.11	4.34	7.03	8.11	4.03	1.43	0.15	0.02	1.65	nd	101.15	0.76	0.81	1.86
1atm-96-3C	64.21	0.52	18.50	0.03	0.99	2.11	3.52	4.60	5.30	0.25	0.02	0.97	nd	101.02	0.94	0.57	1.09
1atm-97-2A	72.03	0.03	14.11	0.03	0.05	0.98	0.31	5.12	5.21	0.02	1.21	0.41	nd	99.51	0.96	0.60	0.49
1atm-95-1A	76.57	0.01	13.13	0.01	0.00	0.01	0.03	2.71	7.63	0.01	0.02	0.25	nd	100.38	1.03	0.35	0.19
1atm-95-1C	75.12	0.01	12.66	0.01	0.00	0.02	0.01	2.42	7.88	0.01	0.02	0.12	nd	98.28	1.01	0.32	0.18
1atm-95-3H	77.4	0.01	12.03	0.01	0.00	0.01	0.04	3.94	5.32	0.01	0.01	0.23	nd	99.01	0.98	0.53	0.22
1atm-95-4	77.87	0.01	12.35	0.01	0.01	0.01	0.02	4.60	4.50	0.01	0.02	0.24	nd	99.65	0.99	0.61	0.24
1atm-96-2B	70.41	0.01	16.76	0.01	0.01	0.03	0.02	5.96	6.21	0.01	0.02	0.34	nd	99.79	1.01	0.59	0.32
1atm-96-2C	70.14	0.06	15.50	0.03	0.05	0.94	0.20	4.45	7.08	0.01	0.85	0.36	nd	99.67	1.01	0.49	0.43
1atm-96-2A	62.2	0.42	19.80	0.02	0.25	1.71	4.06	5.75	4.22	0.01	0.01	0.97	nd	99.42	0.92	0.67	0.95
CS-13-18A	66.90	0.01	16.89	0.00	0.03	0.50	0.53	4.85	7.64	0.02	0.01	0.45	0.002	97.83	1.04	0.49	0.39
CS-13-18B	66.20	0.01	17.79	0.01	0.08	0.41	0.81	5.44	6.87	0.07	0.01	0.47	0.02	98.17	1.09	0.55	0.45
1-12-16A	59.09	0.79	18.23	0.08	3.79	3.12	6.63	4.02	1.04	0.15	0.01	2.21	0.01	99.17	0.92	0.85	2.04
1-12-16B	49.45	0.97	17.93	0.16	4.68	4.85	10.28	2.21	2.21	0.88	0.18	1.69	0.002	95.49	0.72	0.60	1.82
1-12-16C	66.87	0.34	17.31	0.11	1.38	1.56	3.98	4.73	1.66	0.20	0.07	1.38	0.002	99.59	1.03	0.81	1.22
1-02-12A	58.13	0.14	19.32	0.15	0.22	2.04	1.73	8.02	7.03	0.02	0.71	0.77	nd	98.28	0.81	0.63	0.76
1-02-19A	58.21	0.14	19.63	0.15	0.26	1.96	1.76	7.98	6.97	0.02	0.67	0.72	nd	98.47	0.82	0.64	0.81
1-02-12C	57.98	0.14	19.51	0.15	0.23	1.98	1.71	8.17	7.21	0.02	0.69	0.86	nd	98.65	0.80	0.63	0.78
1-99-3A	48.05	1.11	17.21	0.11	4.02	6.51	10.03	3.02	7.18	0.90	0.22	1.44	nd	99.8	0.56	0.39	1.73
1-95-10D	72.11	0.03	13.93	0.03	0.05	1.02	0.31	5.11	4.87	0.02	1.21	0.42	nd	99.11	0.98	0.61	0.50
1-95-10G	72.06	0.03	14.02	0.03	0.05	1.03	0.33	5.09	5.00	0.02	1.19	0.41	nd	99.26	0.97	0.61	0.50
1-09-14C	69.93	0.45	12.59	0.04	0.27	1.94	2.95	4.22	2.67	0.05	0.06	0.94	0.009	96.12	0.83	0.71	0.78
1-09-15B	67.73	0.30	12.82	0.06	0.18	2.04	5.46	4.49	2.64	0.03	0.02	1.31	0.021	97.11	0.63	0.72	1.10
1-09-15C	70.53	0.31	12.41	0.04	0.18	1.92	3.24	4.66	2.91	0.04	0.16	0.96	0.006	97.36	0.74	0.71	0.83
1-95-9E	72.15	0.27	12.22	0.03	0.14	0.78	0.35	3.45	7.29	0.01	0.15	0.39	0.002	97.23	0.86	0.42	0.36
1-95-9A	70.39	0.25	12.18	0.05	0.13	0.86	0.54	5.26	8.96	0.03	0.02	0.46	0.01	99.13	0.63	0.47	0.48
1-95-9B	72.34	0.24	12.31	0.03	0.15	0.81	0.33	3.33	7.63	0.01	0.14	0.36	0.004	97.68	0.86	0.40	0.36
1-95-9C	73.21	0.25	12.24	0.02	0.13	0.81	0.32	3.44	6.89	0.01	0.11	0.35	0.003	97.78	0.89	0.43	0.35
1-95-9G	71.42	0.04	13.31	0.01	0.02	0.64	0.14	4.17	6.94	0.01	0.86	0.41	0.004	97.97	0.91	0.48	0.40
1-09-16A	70.78	0.40	14.84	0.04	0.74	0.42	4.76	4.62	2.25	0.10	0.10	1.13	0.009	100.19	0.79	0.76	1.11

1-09-16D	69.67	0.43	14.68	0.03	0.76	1.38	2.49	5.12	3.74	0.09	0.02	0.95	0.005	99.37	0.86	0.68	0.88
1-94-22D	73.96	0.02	15.79	0.01	0.01	0.01	0.01	4.95	4.03	0.01	0.02	0.50	0.002	99.32	1.26	0.65	0.58
1-94-22A	76.89	0.00	12.57	0.01	0.02	0.02	0.03	4.76	5.11	0.03	0.01	0.23	0.005	99.68	0.94	0.59	0.28
1-94-22C	76.79	0.01	13.37	0.01	0.01	0.01	0.13	4.43	4.26	0.01	0.01	0.26	0.003	99.3	1.10	0.61	0.27
1-94-22B	76.85	0.02	11.99	0.03	0.01	0.01	0.13	4.46	4.19	0.01	0.01	0.24	0.002	97.95	0.99	0.62	0.27
1-94-22E	74.19	0.01	11.38	0.01	0.03	0.03	0.01	5.9	7.65	0.02	0.01	0.31	0.003	99.55	0.63	0.54	0.36
1-94-23D	73.68	0.02	15.62	0.01	0.01	0.01	0.01	4.84	4.47	0.03	0.02	0.42	0.002	99.14	1.22	0.62	0.53
1-94-23F	76.18	0.03	13.16	0.02	0.01	0.03	0.14	4.72	4.56	0.01	0.01	0.35	0.002	99.22	1.02	0.61	0.28
1-94-23H	76.87	0.01	12.47	0.02	0.03	0.01	0.16	4.95	4.67	0.03	0.01	0.20	0.004	99.43	0.92	0.62	0.30
1-94-23C	75.79	0.02	12.92	0.03	0.02	0.01	0.03	4.92	5.41	0.01	0.01	0.20	0.005	99.37	0.92	0.58	0.29
1-94-23B	73.34	0.01	11.79	0.02	0.01	0.01	0.01	6.68	7.32	0.03	0.03	0.38	0.004	99.63	0.62	0.58	0.38
2012-H5-6	47.21	1.62	16.21	0.15	8.91	8.79	9.69	2.54	1.12	0.51	0.03	3.42	0.006	100.21	0.70	0.78	2.87
2012-H5-4	51.98	0.93	21.81	0.11	4.01	6.03	6.57	2.51	1.10	0.01	0.10	2.64	0.008	97.80	1.26	0.78	1.90
2012-H5-2	56.97	0.32	23.04	0.12	0.13	2.08	1.03	8.82	4.97	0.06	0.10	0.92	0.004	98.56	1.06	0.73	0.72
2012-H5-5	76.02	0.01	14.03	0.01	0.21	0.02	0.66	3.92	4.72	0.01	0.10	0.71	0.013	100.43	1.10	0.56	0.45
2012-H5-1	50.00	0.81	15.99	0.02	5.62	6.41	10.58	1.42	4.40	0.02	0.04	2.33	0.007	97.65	0.61	0.33	2.77
2012-H5-3	65.89	0.36	17.02	0.12	1.31	2.62	3.97	3.98	1.40	0.19	0.12	1.62	0.004	98.60	1.11	0.81	1.43
1-95-12E	71.22	0.02	15.15	0.03	0.01	0.02	2.61	3.61	5.37	0.01	0.01	0.52	nd	98.58	0.92	0.51	0.60
1-95-12B	70.23	0.02	15.32	0.03	0.01	0.02	1.51	4.11	6.85	0.03	0.01	0.53	nd	98.67	0.91	0.48	0.48
1-97-3A	69.81	0.04	17.16	0.01	0.01	0.03	0.02	4.71	8.14	0.02	0.02	0.26	nd	100.23	1.03	0.47	0.31
1-97-3C	75.34	0.01	13.01	0.04	0.02	0.01	0.01	4.25	5.93	0.02	0.03	0.22	nd	98.89	0.97	0.52	0.26
1-99-1B	54.05	0.92	16.17	0.12	7.01	6.75	6.34	3.25	1.02	0.28	0.01	2.34	0.01	98.26	0.89	0.83	2.47
1-00-18A	49.71	1.06	19.04	0.07	11.5	0.11	12.04	1.38	0.11	0.04	0.01	4.19	nd	99.26	0.78	0.95	4.75
1-00-18B	51.17	1.37	16.93	0.11	9.92	0.03	13.81	1.96	0.17	0.03	0.01	3.89	nd	99.4	0.59	0.95	4.24
1-00-23A	52.51	1.04	19.79	0.07	9.37	0.87	7.95	1.46	0.11	0.03	0.01	3.92	nd	97.13	1.16	0.95	3.62
1-00-23B	54.77	1.19	18.53	0.06	10.81	0.11	7.97	1.42	0.12	0.04	0.01	3.82	nd	98.85	1.09	0.95	3.83
1-00-23C	55.97	0.92	20.68	0.03	6.40	0.11	8.56	1.86	0.16	0.03	0.01	3.20	nd	97.93	1.10	0.95	3.17
1-00-23D	54.91	0.95	20.41	0.05	7.81	0.11	9.02	1.79	0.15	0.02	0.01	3.37	nd	98.6	1.05	0.95	3.30
1-00-23E	55.44	1.23	18.01	0.07	10.08	0.12	8.79	1.67	0.15	0.02	0.01	3.63	nd	99.22	0.95	0.94	3.66
1-00-28A	56.86	1.49	15.8	0.05	7.61	2.67	6.24	0.93	0.06	0.05	0.04	3.49	nd	95.29	1.22	0.96	3.23
1-00-28B	59.56	1.32	16.95	0.04	6.86	0.49	8.26	1.81	0.17	0.02	0.27	3.08	nd	98.83	0.93	0.94	3.49
1-00-28C	59.07	1.56	15.98	0.04	7.45	0.41	8.07	1.39	0.14	0.03	0.24	3.34	nd	97.72	0.93	0.94	3.71
1-00-28D	62.27	1.36	16.45	0.05	4.98	0.45	7.36	1.71	0.17	0.02	0.29	2.77	nd	97.88	1.00	0.94	2.40
1-00-28F	59.65	1.55	15.44	0.03	6.97	2.46	5.71	0.89	0.06	0.02	0.06	3.39	nd	96.23	1.29	0.96	3.65
1-01-35B	61.11	1.27	15.45	0.05	4.54	0.85	7.35	3.15	0.3	0.02	0.02	2.56	nd	96.67	0.82	0.94	2.25

1-01-35C	61.96	1.85	17.76	0.07	3.82	0.70	6.51	3.85	0.36	0.01	0.02	2.34	nd	99.25	0.96	0.94	2.00
1-07-13A	64.70	0.48	14.10	0.04	0.72	3.27	1.95	5.67	4.34	0.24	0.04	1.19	0.001	96.73	0.80	0.67	1.04
1-07-13B	65.62	0.45	14.19	0.02	0.73	2.52	1.84	5.21	4.24	0.12	0.02	1.03	0.002	95.99	0.86	0.65	0.95
1-00-32B	55.33	1.18	18.61	0.02	8.51	0.26	5.54	1.15	0.07	0.03	0.08	2.65	nd	93.43	1.54	0.96	2.32
1-00-32C	52.31	1.15	18.63	0.01	10.56	0.12	7.45	1.39	0.10	0.05	0.12	2.89	nd	94.78	1.17	0.95	3.07
1-02-11A	57.85	0.17	20.47	0.15	0.15	1.94	1.62	7.81	7.57	0.02	0.76	0.84	nd	99.35	0.85	0.61	0.91
1-07-05	57.06	0.13	21.01	0.15	0.32	2.00	1.89	8.36	6.54	0.03	0.62	0.95	0.009	99.06	0.87	0.66	1.01
1-07-06	55.47	0.11	19.92	0.11	0.16	1.73	1.49	8.88	6.95	0.02	0.61	0.83	0.005	96.27	0.80	0.66	0.93
1-94-17A	63.91	0.05	14.84	0.06	0.06	0.20	0.06	5.22	5.25	0.01	7.83	1.27	0.002	98.76	1.03	0.60	1.30
1-94-17B	73.14	0.26	12.74	0.08	0.14	1.19	0.66	3.45	6.34	0.01	0.22	0.44	0.004	98.67	0.93	0.45	0.50
1-10-07A	72.51	0.02	12.07	0.01	0.01	0.04	0.00	5.57	7.22	0.00	0.01	0.35	0.012	97.55	0.71	0.54	0.38
1-96-13E	75.07	0.01	11.23	0.03	0.01	0.01	0.02	5.77	7.44	0.01	0.01	0.37	0.005	99.98	0.64	0.54	0.40
1-96-13D	77.71	0.02	10.39	0.01	0.02	0.03	0.01	6.18	8.03	0.02	0.01	0.42	0.004	102.9	0.55	0.54	0.43
1-99-15	45.22	1.14	11.06	0.13	5.89	10.6	11.96	0.75	0.50	1.14	0.13	4.11	nd	92.63	0.47	0.70	3.62
1-94-1D	71.42	0.05	14.01	0.11	0.07	1.14	0.42	4.29	3.99	0.02	1.23	0.57	0.004	97.32	1.15	0.62	0.59
1-03-09B	56.17	0.15	18.14	0.08	0.15	1.22	4.56	5.50	5.20	0.02	0.67	1.21	nd	93.07	0.79	0.62	1.17
1-99-12	40.71	0.69	14.50	0.10	7.73	8.79	5.31	0.68	1.35	8.62	0.03	3.86	nd	92.37	1.18	0.43	3.52
1-00-19B	30.17	0.42	9.39	0.26	5.21	21.98	16.9	0.63	0.11	6.03	0.17	5.91	nd	97.18	0.29	0.90	6.68
1-96-1B	76.71	0.01	11.78	0.02	0.02	0.03	0.03	4.16	4.50	0.02	0.01	0.25	nd	97.54	1.00	0.58	0.32
1-96-1E	72.05	0.02	10.78	0.02	0.01	0.02	0.02	4.33	6.07	0.03	0.04	0.31	nd	93.7	0.79	0.52	0.30
1-96-1D	76.62	0.02	12.15	0.01	0.02	0.03	0.04	3.99	3.75	0.04	0.01	0.24	nd	96.92	1.14	0.62	0.29
1-96-1F	76.09	0.01	11.99	0.01	0.01	0.01	0.01	4.76	6.11	0.01	0.03	0.40	nd	99.44	0.83	0.54	0.36
1-96-1A	75.63	0.03	12.08	0.03	0.01	0.03	0.02	4.07	4.16	0.03	0.01	0.24	nd	96.34	1.08	0.60	0.30
1-96-1C	77.19	0.02	12.19	0.04	0.03	0.01	0.01	3.99	6.26	0.02	0.02	0.41	nd	100.19	0.91	0.49	0.31
2012-H2-1	59.39	0.33	23.37	0.12	0.17	2.14	1.02	9.02	4.95	0.05	0.11	1.15	0.003	101.82	1.06	0.73	1.10
2012-H2-2	52.03	0.94	22.45	0.11	3.98	7.09	6.50	2.59	1.21	0.01	0.02	2.89	0.002	99.82	1.29	0.76	2.39
2012-H2-3	48.27	1.75	16.75	0.18	6.15	8.52	10.33	3.13	1.46	0.54	0.09	3.12	0.005	100.30	0.66	0.77	2.91
2012-H2-4	49.47	0.89	15.61	0.02	5.56	7.10	10.68	1.44	5.53	0.01	0.03	2.45	0.003	98.79	0.56	0.28	2.06
2012-H2-5	64.20	0.34	16.94	0.08	1.28	2.91	3.84	4.60	1.53	0.18	0.09	1.83	0.01	97.83	1.04	0.82	1.75
2012-H2-6	74.30	0.03	13.92	0.01	0.17	0.03	0.71	4.14	5.02	0.01	0.04	0.61	0.01	99.00	1.03	0.56	0.55
1-95-8B	75.61	0.02	12.96	0.01	0.01	0.04	0.02	4.11	4.45	0.01	0.02	0.35	0.002	97.61	1.12	0.58	0.35
1-96-5A	76.02	0.01	12.37	0.01	0.01	0.01	0.02	4.72	5.41	0.01	0.01	0.32	0.006	98.92	0.91	0.57	0.39
1-96-5E	78.57	0.01	14.15	0.03	0.03	0.01	0.01	8.02	0.02	0.02	0.01	0.47	0.01	101.30	1.07	1.00	0.53
1-96-5F	75.95	0.01	11.39	0.01	0.02	0.03	0.01	0.04	11.02	0.01	0.01	0.15	0.002	98.66	0.95	0.01	0.18
1-95-11A	75.84	0.03	13.15	0.02	0.01	0.02	0.01	3.97	5.69	0.01	0.02	0.37	nd	99.14	1.03	0.51	0.35

1-95-11E2	73.73	0.02	11.74	0.02	0.02	0.01	0.01	4.27	5.37	0.01	0.01	0.36	nd	95.57	0.91	0.55	0.36
1-95-11E	73.98	0.03	12.21	0.01	0.03	5.70	0.01	4.15	5.74	0.02	0.06	0.77	nd	102.7	0.94	0.52	0.86
1-95-11B2	73.08	0.02	12.52	0.01	0.02	0.02	0.01	3.73	5.70	0.01	0.01	0.35	nd	95.48	1.02	0.50	0.34
1-97-10A	76.71	0.02	13.31	0.02	0.01	0.05	0.02	3.98	6.37	0.03	0.01	0.54	nd	101.07	0.99	0.49	0.37
1-97-10B	76.27	0.02	13.41	0.01	0.02	0.02	0.01	3.96	6.30	0.04	0.02	0.54	nd	100.62	1.00	0.49	0.36
1-97-10C	63.02	0.86	16.5	0.04	1.03	2.14	1.74	5.49	7.03	0.06	0.06	1.15	nd	99.12	0.83	0.54	1.31
2012-H1-1	47.82	1.71	16.46	0.15	6.11	7.91	10.49	3.34	1.60	0.54	0.04	3.21	0.003	99.37	0.63	0.76	3.48
2012-H1-2	51.92	0.92	22.14	0.11	4.07	6.71	6.49	2.60	1.16	0.02	0.1	3.09	0.003	99.33	1.28	0.77	2.88
2012-H1-3	57.21	0.32	22.67	0.09	0.16	2.39	0.96	8.93	5.04	0.03	0.02	1.37	0.003	99.19	1.04	0.73	1.08
2012-H1-5	49.71	0.89	15.64	0.02	5.74	6.70	10.92	1.73	6.02	0.02	0.06	2.21	0.002	99.68	0.53	0.30	2.47
2012-H1-4	74.54	0.02	14.24	0.01	0.19	0.04	0.75	4.41	5.29	0.01	0.04	0.82	0.004	100.38	0.99	0.56	0.69
2012-H3-1	56.71	0.36	22.71	0.12	0.15	1.59	0.95	8.96	5.03	0.03	0.02	1.15	0.01	97.78	1.04	0.73	0.87
2012-H3-2	66.82	0.41	16.21	0.09	1.46	2.25	3.09	4.21	1.54	0.22	0.1	1.74	0.005	98.15	1.14	0.81	1.64
2012-H3-3	75.29	0.04	13.52	0.02	0.19	0.04	0.56	3.75	4.96	0.05	0.01	0.79	0.01	99.22	1.08	0.53	0.52
2012-H3-4	70.31	0.02	16.51	0.01	0.24	0.04	0.88	5.06	5.74	0.01	0.03	0.74	0.01	99.59	1.02	0.57	0.71
2012-H4-2	48.63	0.84	15.46	0.02	5.53	7.05	10.52	1.56	5.91	0.01	0.01	3.02	0.008	98.56	0.55	0.29	2.82
2012-H4-3	66.21	0.33	16.91	0.11	1.31	2.86	3.95	4.27	1.61	0.19	0.02	2.18	0.007	99.95	1.06	0.80	2.34
2012-H4-4	59.37	0.33	22.51	0.11	0.16	2.23	0.97	8.24	4.96	0.04	0.05	1.45	0.007	100.42	1.09	0.72	1.40
2012-H4-5	50.91	0.88	21.66	0.12	3.92	6.32	6.36	2.56	1.11	0.01	0.03	3.48	0.01	97.36	1.27	0.78	3.23
2012-H4-6	75.79	0.01	14.69	0.01	0.21	0.07	0.79	4.27	4.97	0.01	0.05	0.79	0.005	101.66	1.06	0.57	0.80

[a]All iron expressed as FeO.
[b]Molar (Al_2O_3/CaO+Na_2O+K_2O) of the melt.
[c]Molar (Na_2O/Na_2O+K_2O) of the melt.
[d]Modeled solubility of Cl in the melt (wt%).
[e]nd = not determined.

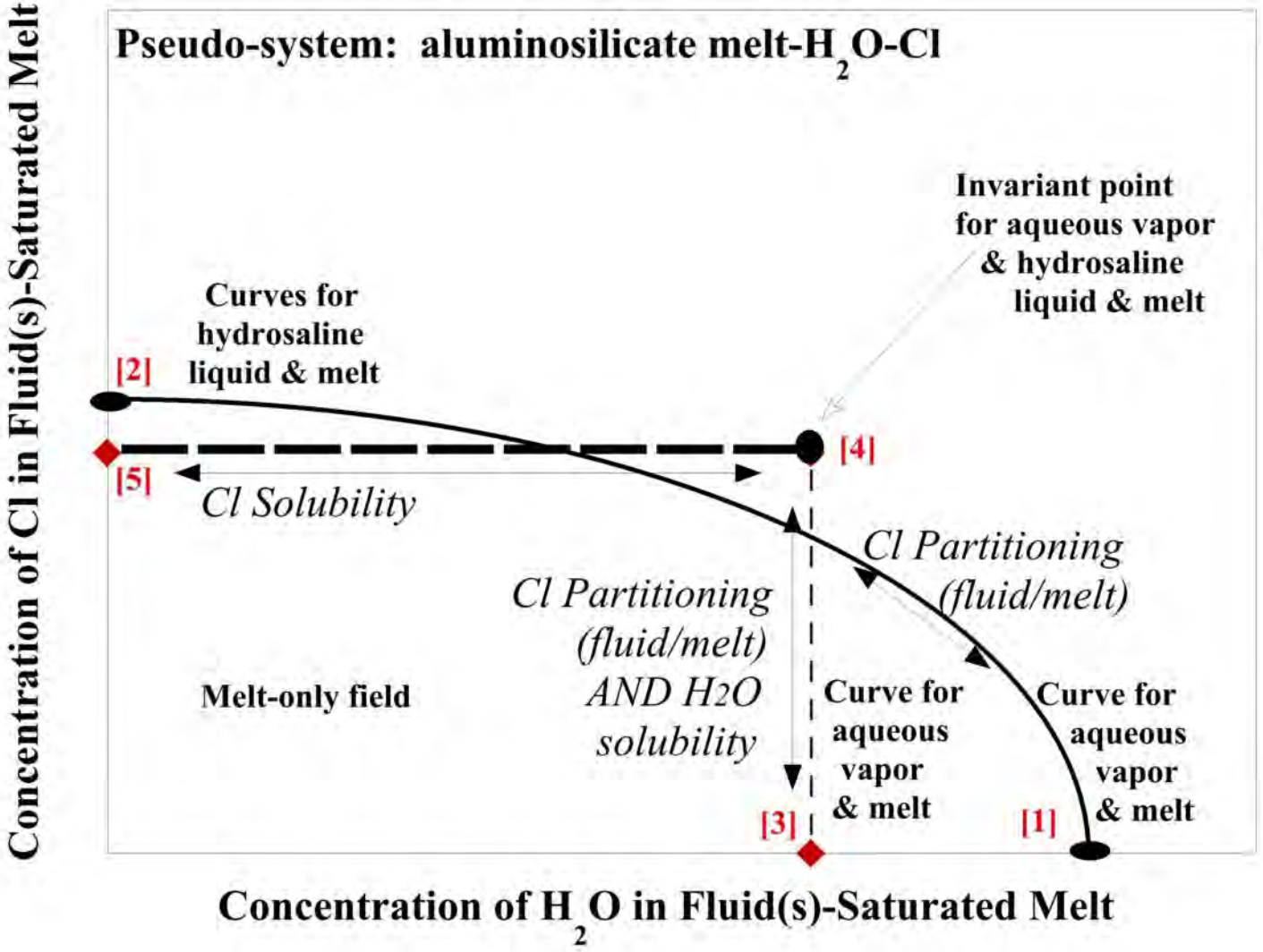
Pseudo-system: aluminosilicate melt-H2O-Cl
Concentration of Cl in Fluid(s)-Saturated Melt
Concentration of H2O in Fluid(s)-Saturated Melt
Invariant point for aqueous vapor & hydrosaline liquid & melt
Curves for hydrosaline liquid & melt
[2]
[4]
[5]
Cl Solubility
Cl Partitioning (fluid/melt)
Cl Partitioning (fluid/melt) AND H2O solubility
Melt-only field
Curve for aqueous vapor & melt
Curve for aqueous vapor & melt
[3]
[1]

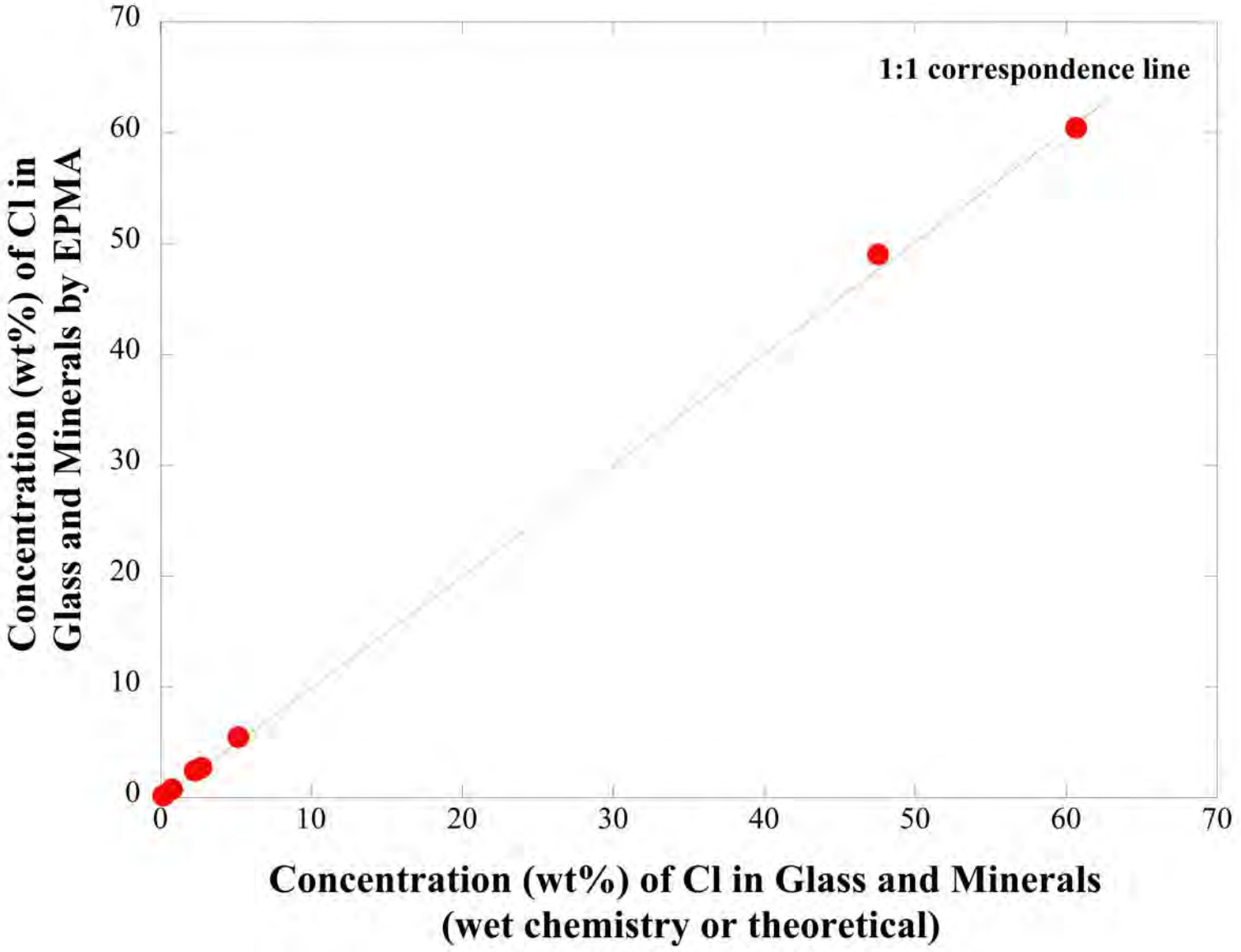
1:1 correspondence line
Concentration (wt%) of Cl in Glass and Minerals by EPMA
Concentration (wt%) of Cl in Glass and Minerals (wet chemistry or theoretical)
0
10
20
30
40
50
60
70

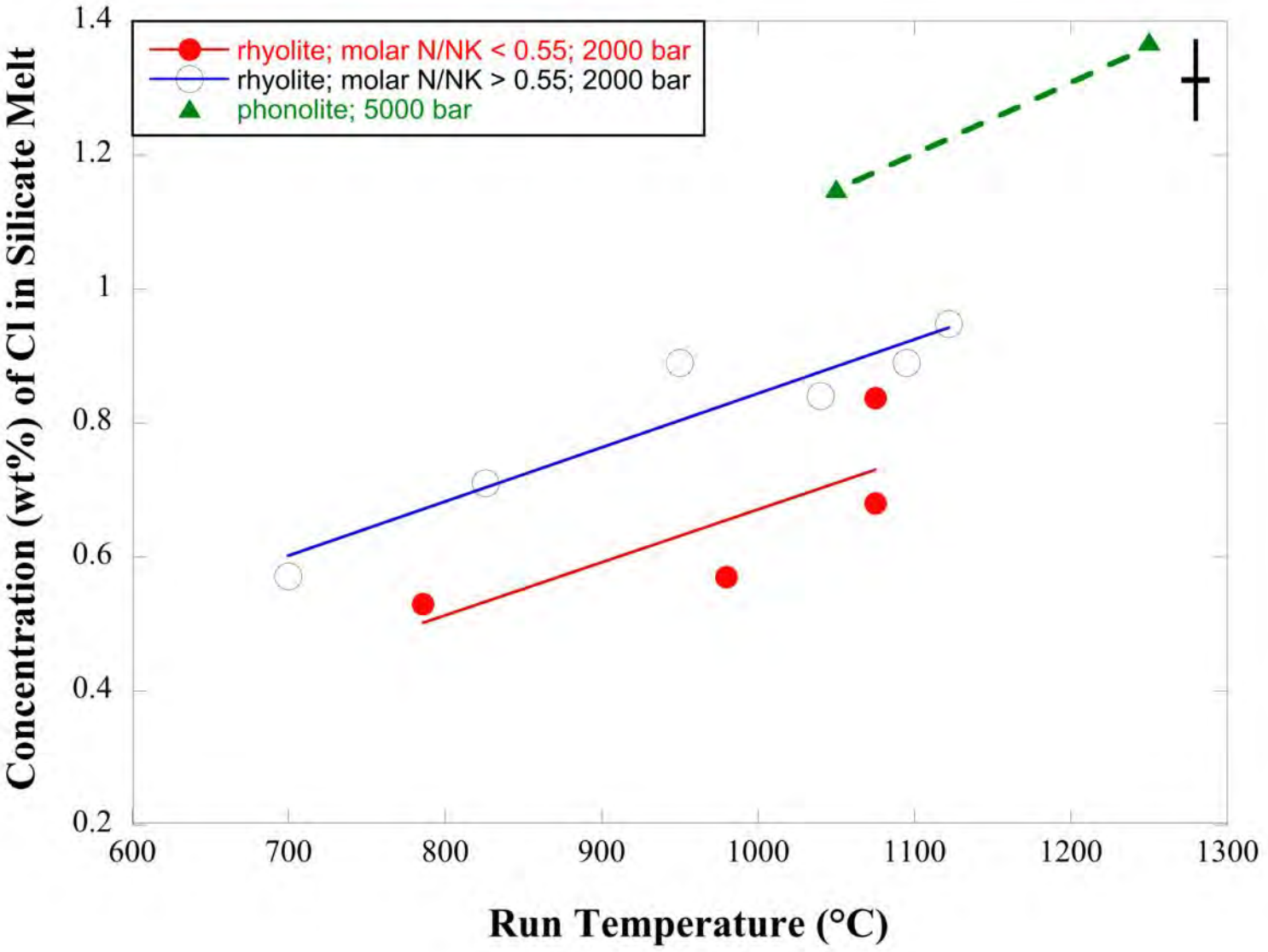
rhyolite; molar N/NK < 0.55; 2000 bar
rhyolite; molar N/NK > 0.55; 2000 bar
phonolite; 5000 bar
Concentration (wt%) of Cl in Silicate Melt
Run Temperature (°C)
1.4
1.2
1
0.8
0.6
0.4
0.2
600
700
800
900
1000
1100
1200
1300

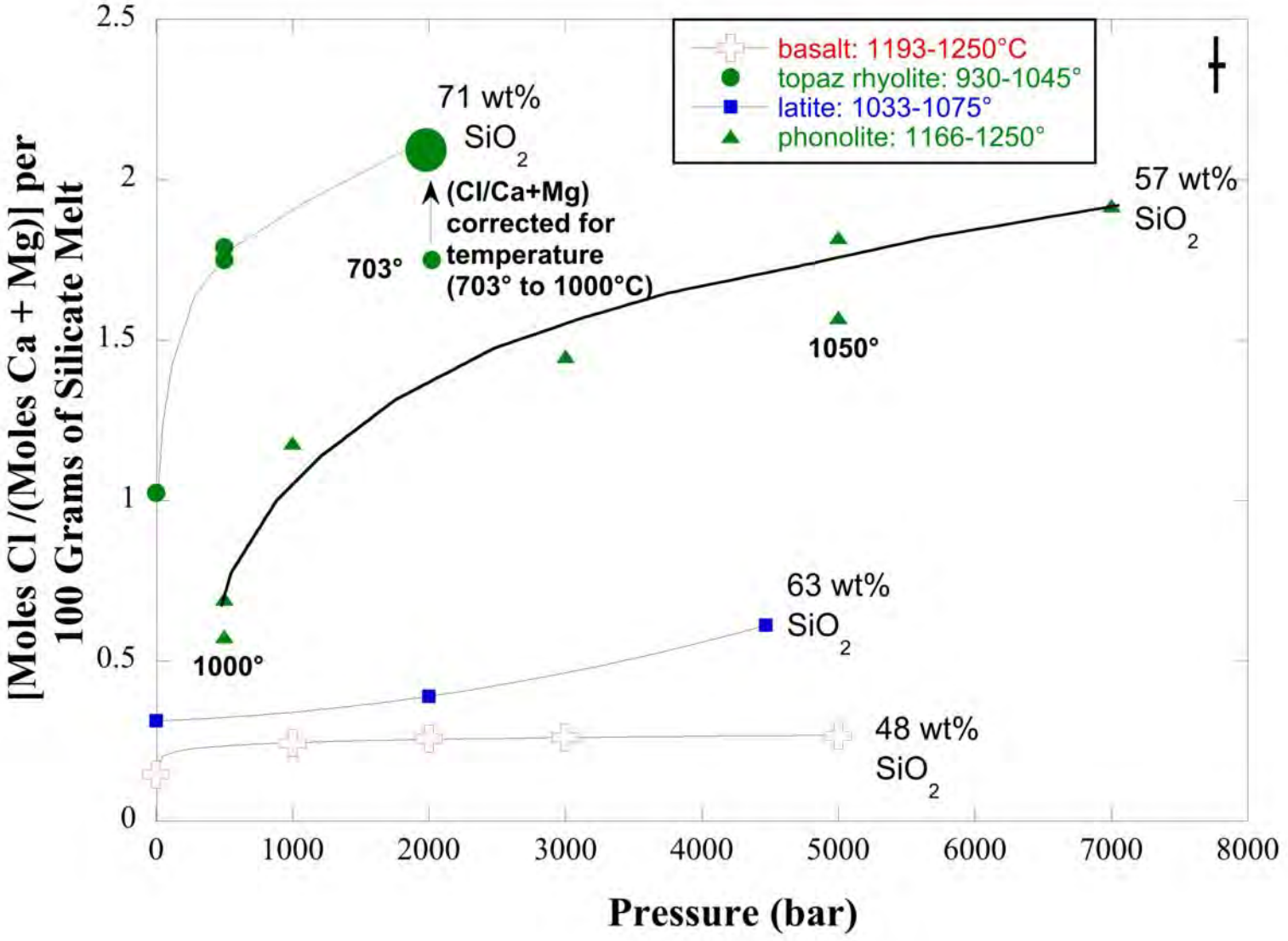
basalt: 1193-1250°C
topaz rhyolite: 930-1045°
latite: 1033-1075°
phonolite: 1166-1250°
71 wt% SiO2
(Cl/Ca+Mg) corrected for temperature (703° to 1000°C)
703°
57 wt% SiO2
1050°
1000°
63 wt% SiO2
48 wt% SiO2
[Moles Cl /(Moles Ca + Mg)] per 100 Grams of Silicate Melt
Pressure (bar)
0
0.5
1
1.5
2
2.5
0
1000
2000
3000
4000
5000
6000
7000
8000

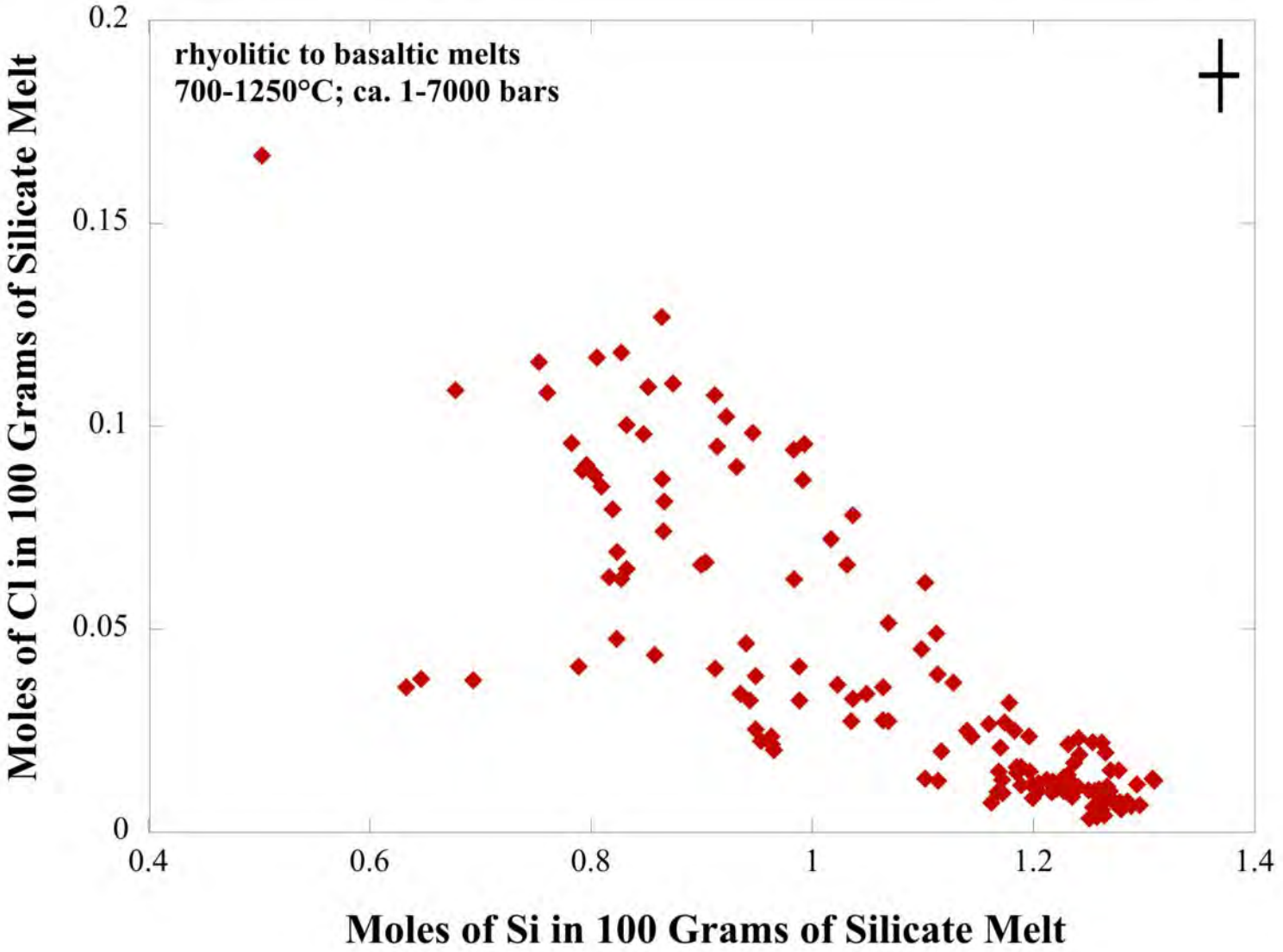
rhyolitic to basaltic melts
700-1250°C; ca. 1-7000 bars
Moles of Cl in 100 Grams of Silicate Melt
0.2
0.15
0.1
0.05
0
0.4
0.6
0.8
1
1.2
1.4
Moles of Si in 100 Grams of Silicate Melt

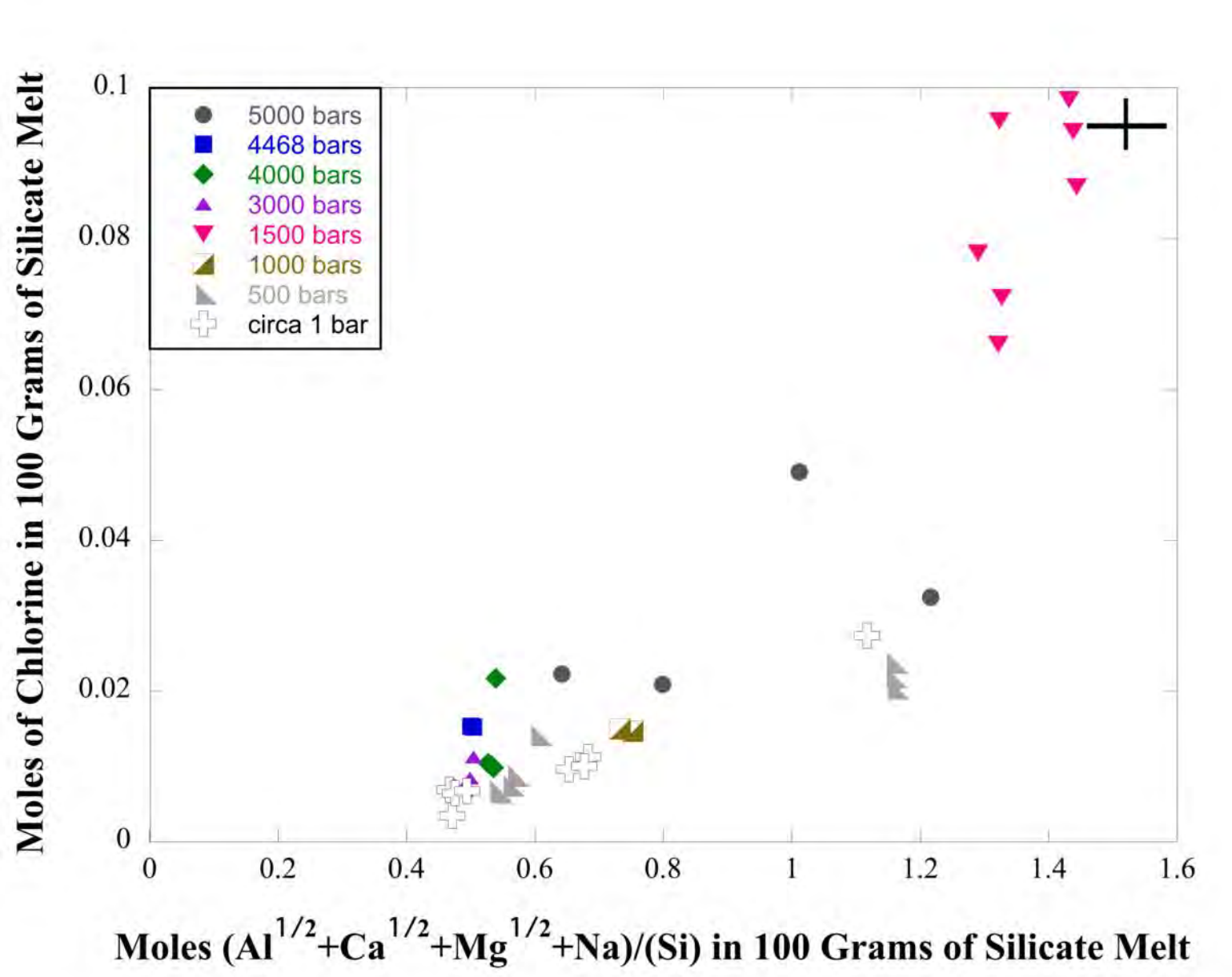
5000 bars
4468 bars
4000 bars
3000 bars
1500 bars
1000 bars
500 bars
circa 1 bar
0.1
0.08
0.06
0.04
0.02
0
0
0.2
0.4
0.6
0.8
1
1.2
1.4
1.6
Moles of Chlorine in 100 Grams of Silicate Melt
Moles (Al1/2+Ca1/2+Mg1/2+Na)/(Si) in 100 Grams of Silicate Melt

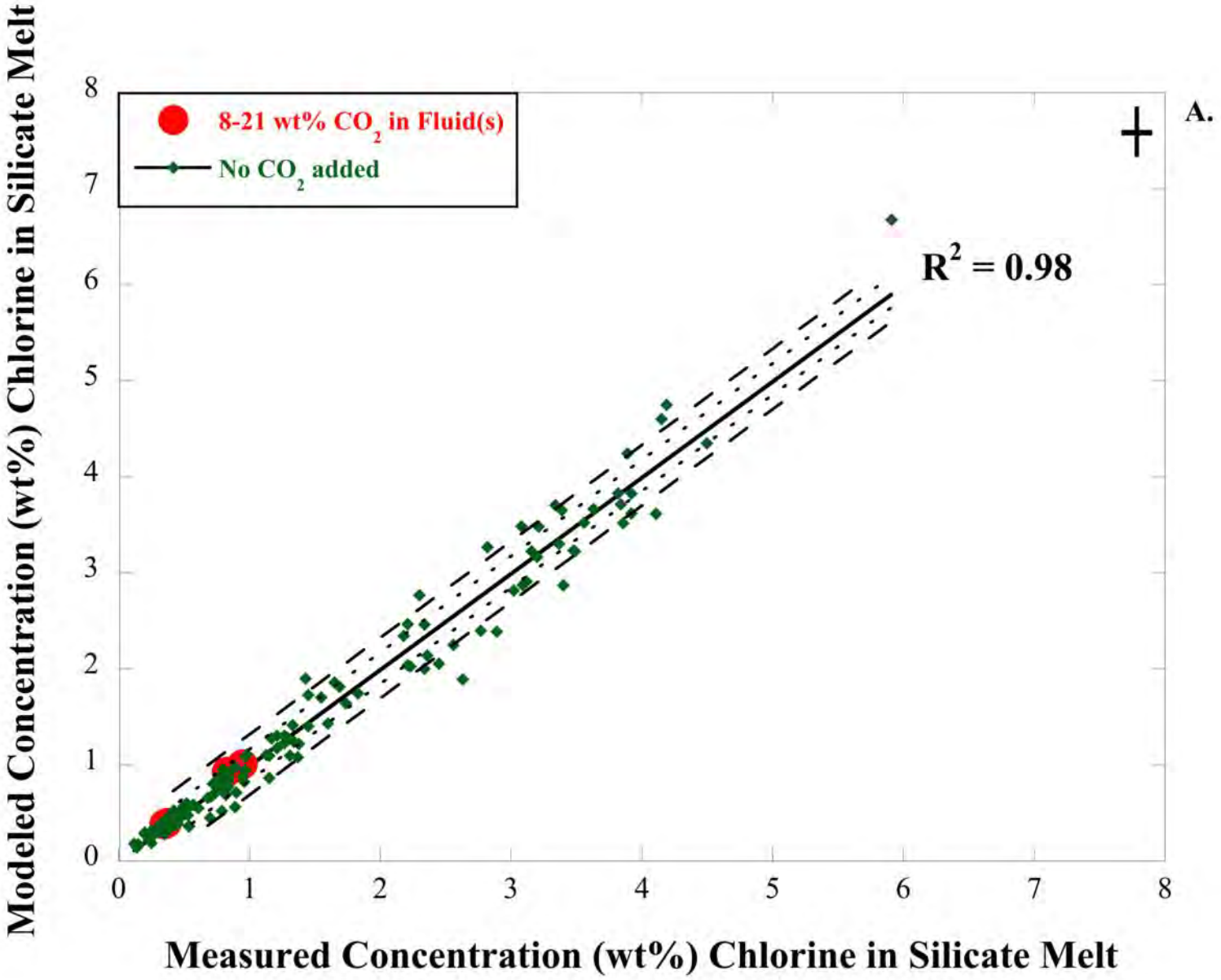
8-21 wt% CO2 in Fluid(s)
No CO2 added
R2 = 0.98
A.
Modeled Concentration (wt%) Chlorine in Silicate Melt
Measured Concentration (wt%) Chlorine in Silicate Melt
0
1
2
3
4
5
6
7
8

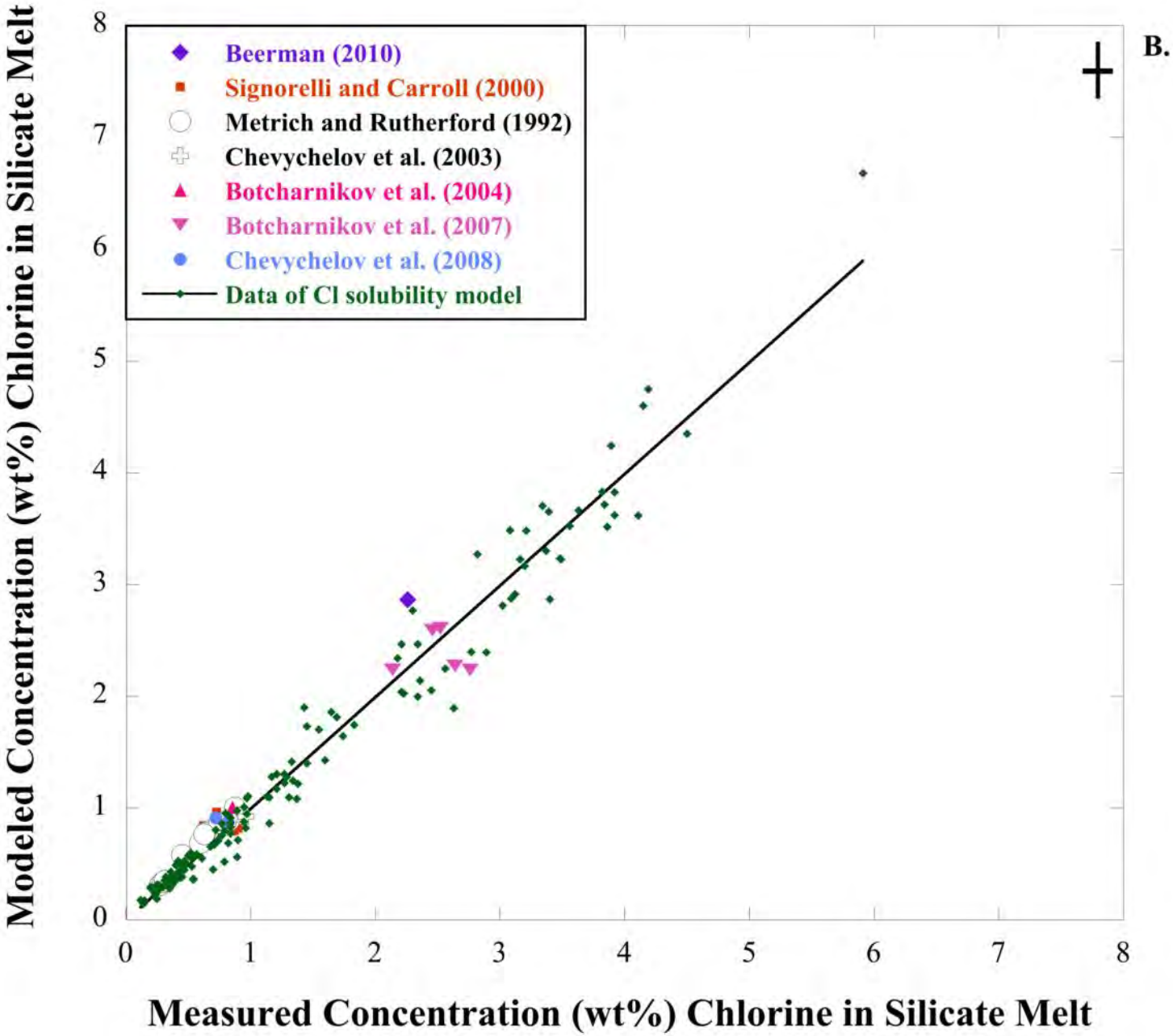
B.
Beerman (2010)
Signorelli and Carroll (2000)
Metrich and Rutherford (1992)
Chevychelov et al. (2003)
Botcharnikov et al. (2004)
Botcharnikov et al. (2007)
Chevychelov et al. (2008)
Data of Cl solubility model
Modeled Concentration (wt%) Chlorine in Silicate Melt
Measured Concentration (wt%) Chlorine in Silicate Melt
0
1
2
3
4
5
6
7
8

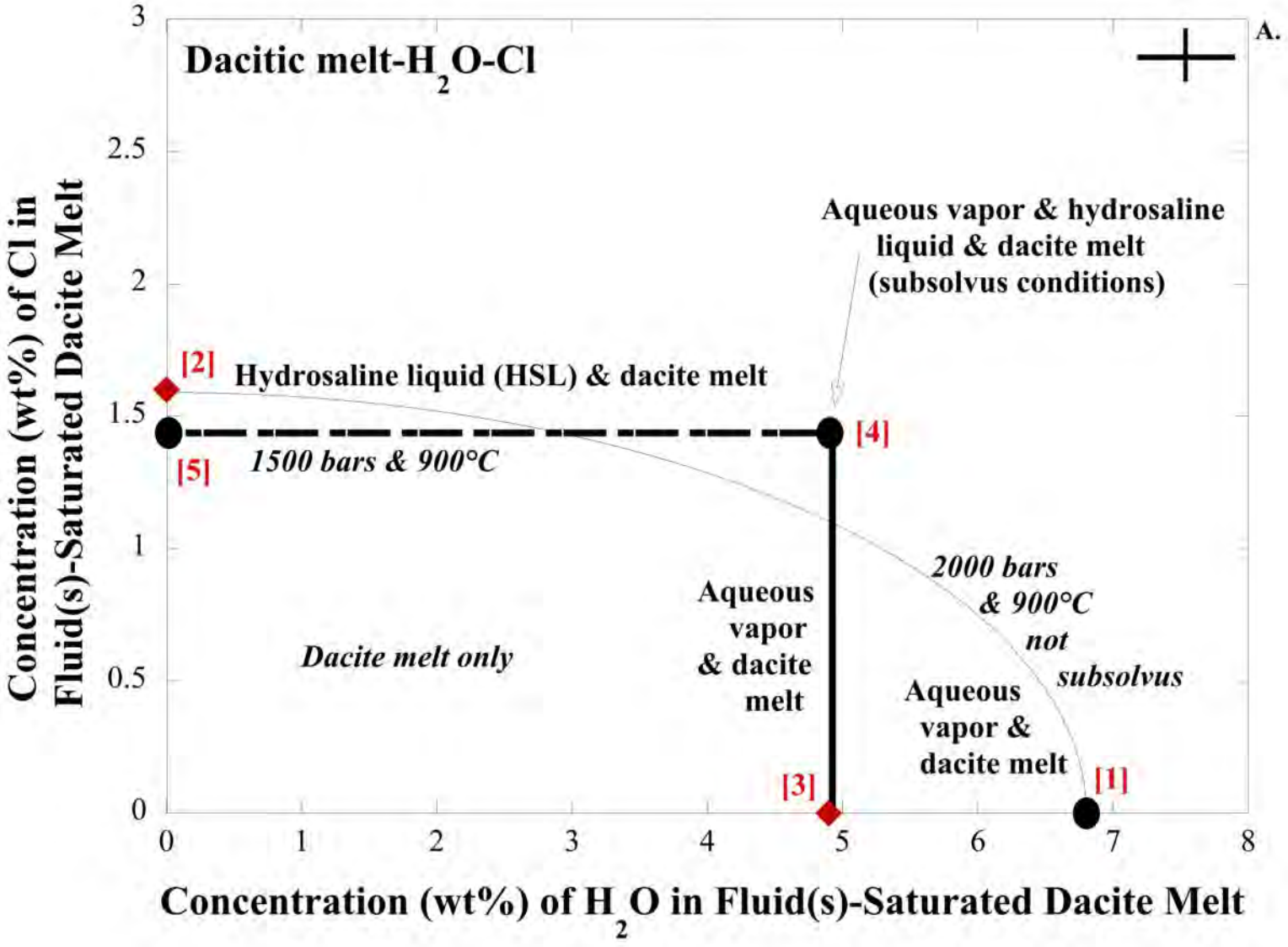
A.
Dacitic melt-H2O-Cl
Concentration (wt%) of Cl in Fluid(s)-Saturated Dacite Melt
Concentration (wt%) of H2O in Fluid(s)-Saturated Dacite Melt
Aqueous vapor & hydrosaline liquid & dacite melt (subsolvus conditions)
[2]
Hydrosaline liquid (HSL) & dacite melt
[4]
[5]
1500 bars & 900°C
2000 bars & 900°C not subsolvus
Dacite melt only
Aqueous vapor & dacite melt
Aqueous vapor & dacite melt
[3]
[1]
0
0.5
1
1.5
2
2.5
3
0
1
2
3
4
5
6
7
8

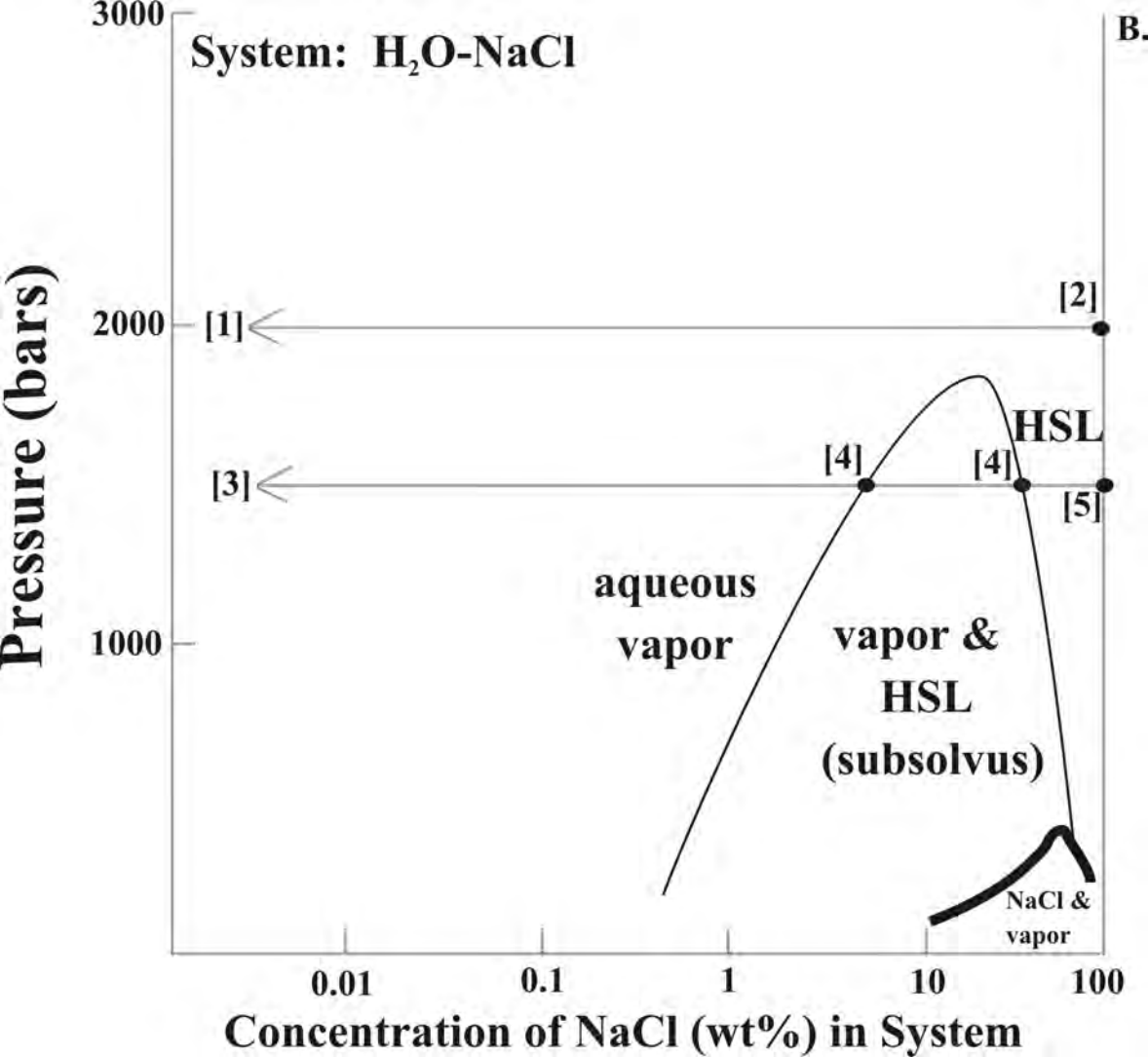
B.
System: H_2O-NaCl
3000
2000
1000
Pressure (bars)
[1]
[2]
[3]
[4]
[4]
[5]
HSL
aqueous
vapor
vapor &
HSL
(subsolvus)
NaCl &
vapor
0.01
0.1
1
10
100
Concentration of NaCl (wt%) in System

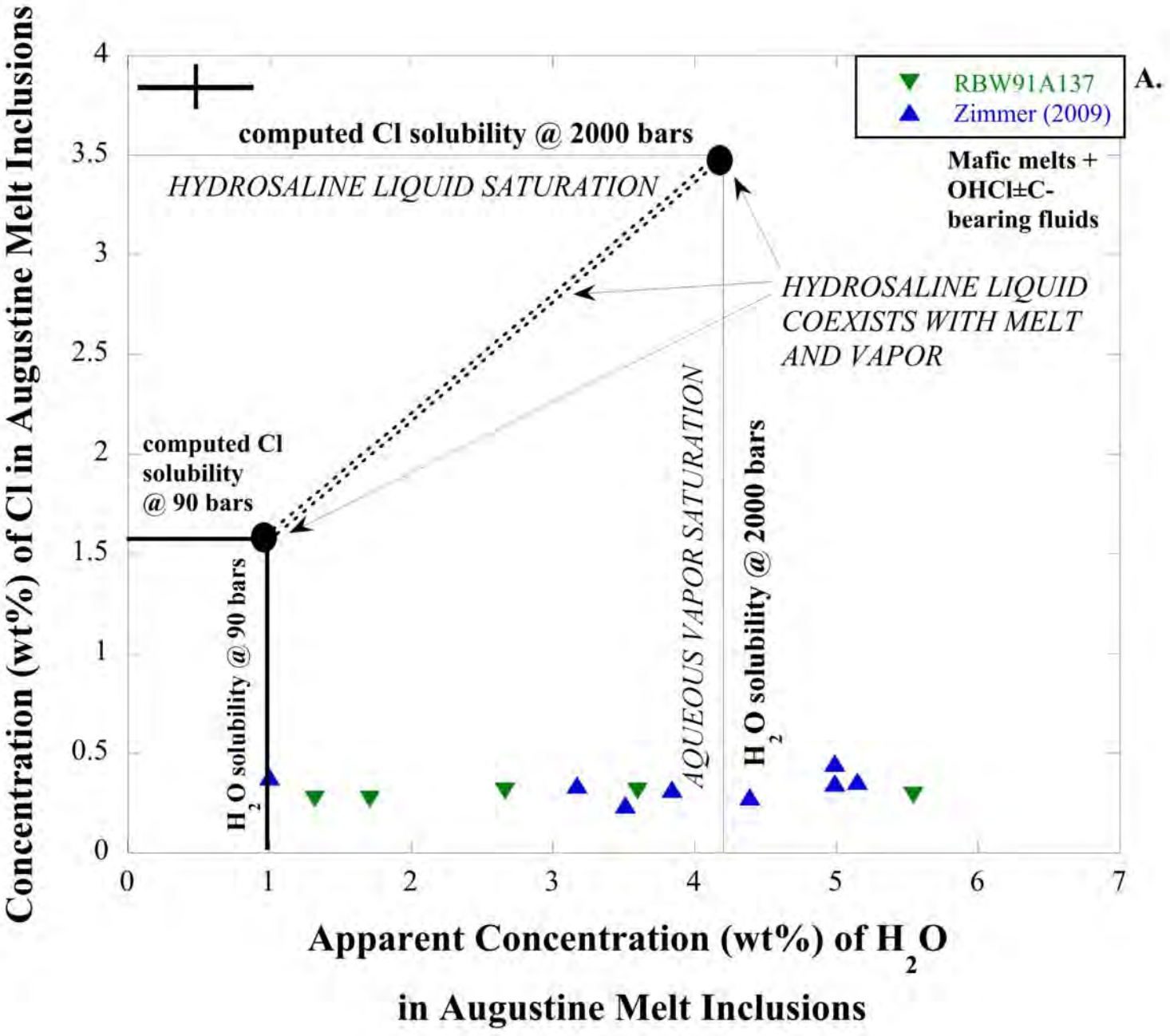
A.
RBW91A137
Zimmer (2009)
Mafic melts + OHCl±C-bearing fluids
computed Cl solubility @ 2000 bars
HYDROSALINE LIQUID SATURATION
HYDROSALINE LIQUID COEXISTS WITH MELT AND VAPOR
computed Cl solubility @ 90 bars
H2O solubility @ 90 bars
AQUEOUS VAPOR SATURATION
H2O solubility @ 2000 bars
Concentration (wt%) of Cl in Augustine Melt Inclusions
Apparent Concentration (wt%) of H2O in Augustine Melt Inclusions
0
0.5
1
1.5
2
2.5
3
3.5
4
0
1
2
3
4
5
6
7

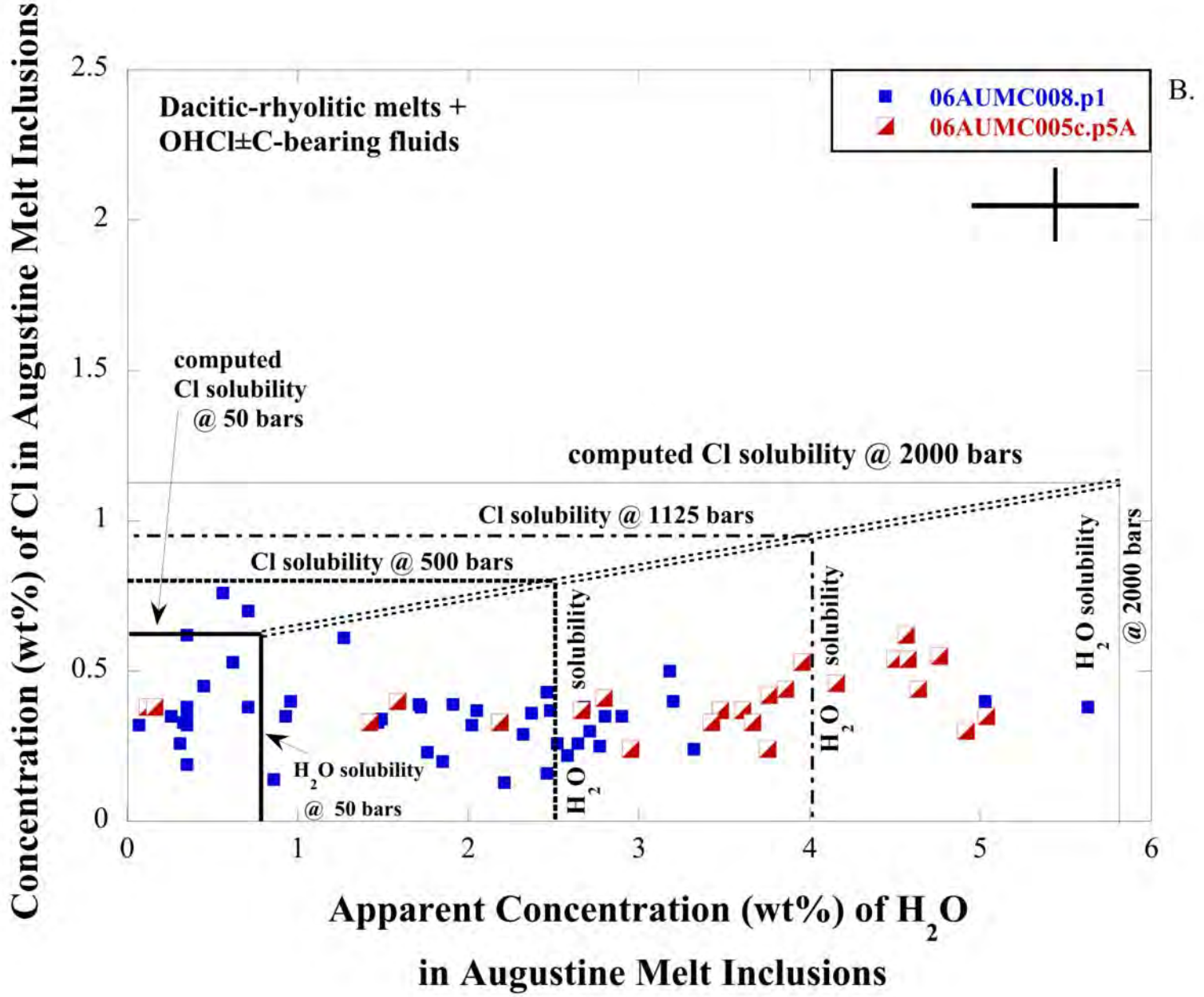
B.
Dacitic-rhyolitic melts +
OHCl±C-bearing fluids
06AUMC008.p1
06AUMC005c.p5A
computed
Cl solubility
@ 50 bars
computed Cl solubility @ 2000 bars
Cl solubility @ 1125 bars
Cl solubility @ 500 bars
H2O solubility
@ 50 bars
H2O solubility
H2O solubility
H2O solubility
@ 2000 bars
Concentration (wt%) of Cl in Augustine Melt Inclusions
Apparent Concentration (wt%) of H2O
in Augustine Melt Inclusions
0
0.5
1
1.5
2
2.5
0
1
2
3
4
5
6

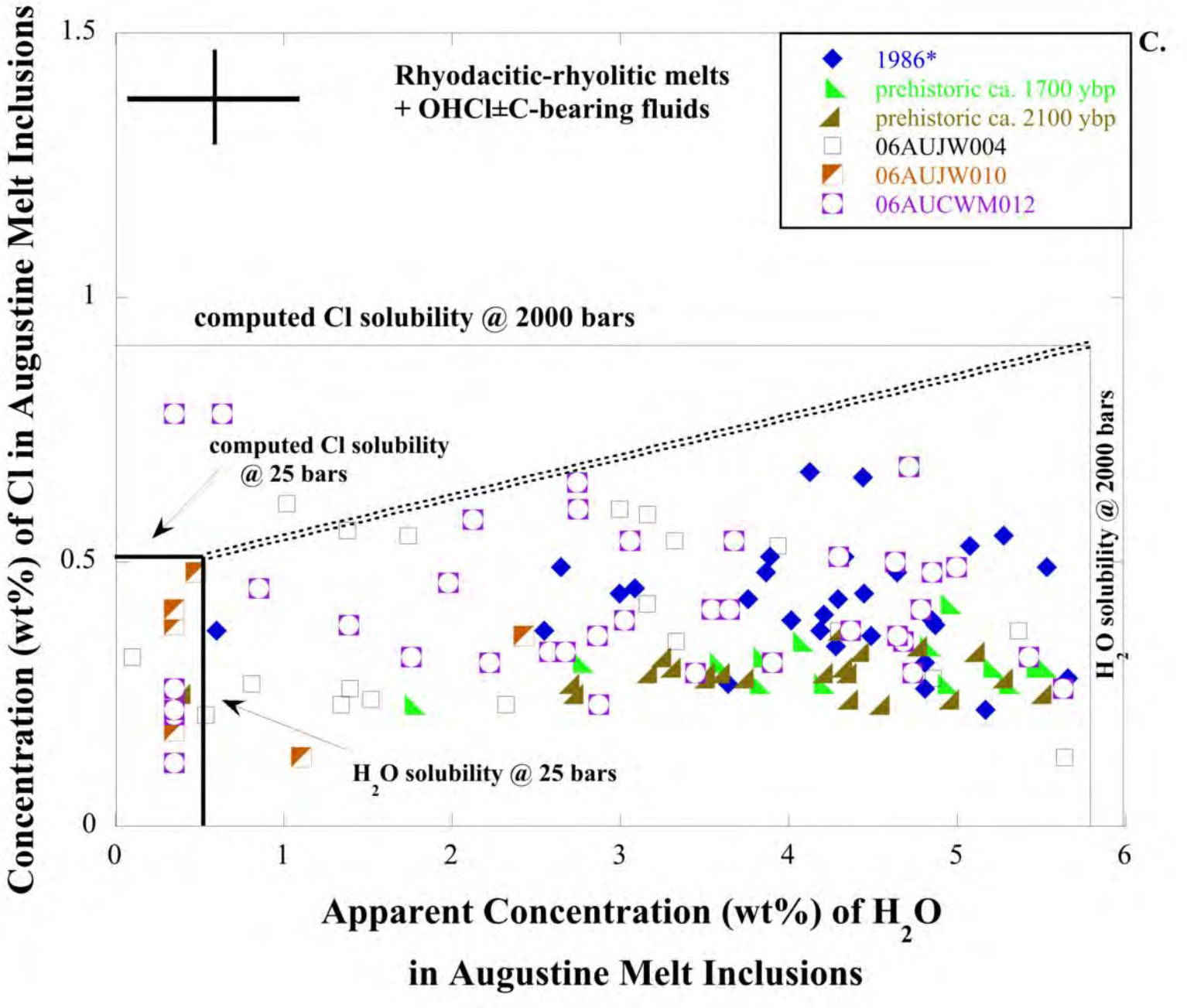
C.
Rhyodacitic-rhyolitic melts
+ OHCl±C-bearing fluids
1986*
prehistoric ca. 1700 ybp
prehistoric ca. 2100 ybp
06AUJW004
06AUJW010
06AUCWM012
computed Cl solubility @ 2000 bars
computed Cl solubility
@ 25 bars
H2O solubility @ 25 bars
H2O solubility @ 2000 bars
Concentration (wt%) of Cl in Augustine Melt Inclusions
Apparent Concentration (wt%) of H2O
in Augustine Melt Inclusions
0
0.5
1
1.5
0
1
2
3
4
5
6

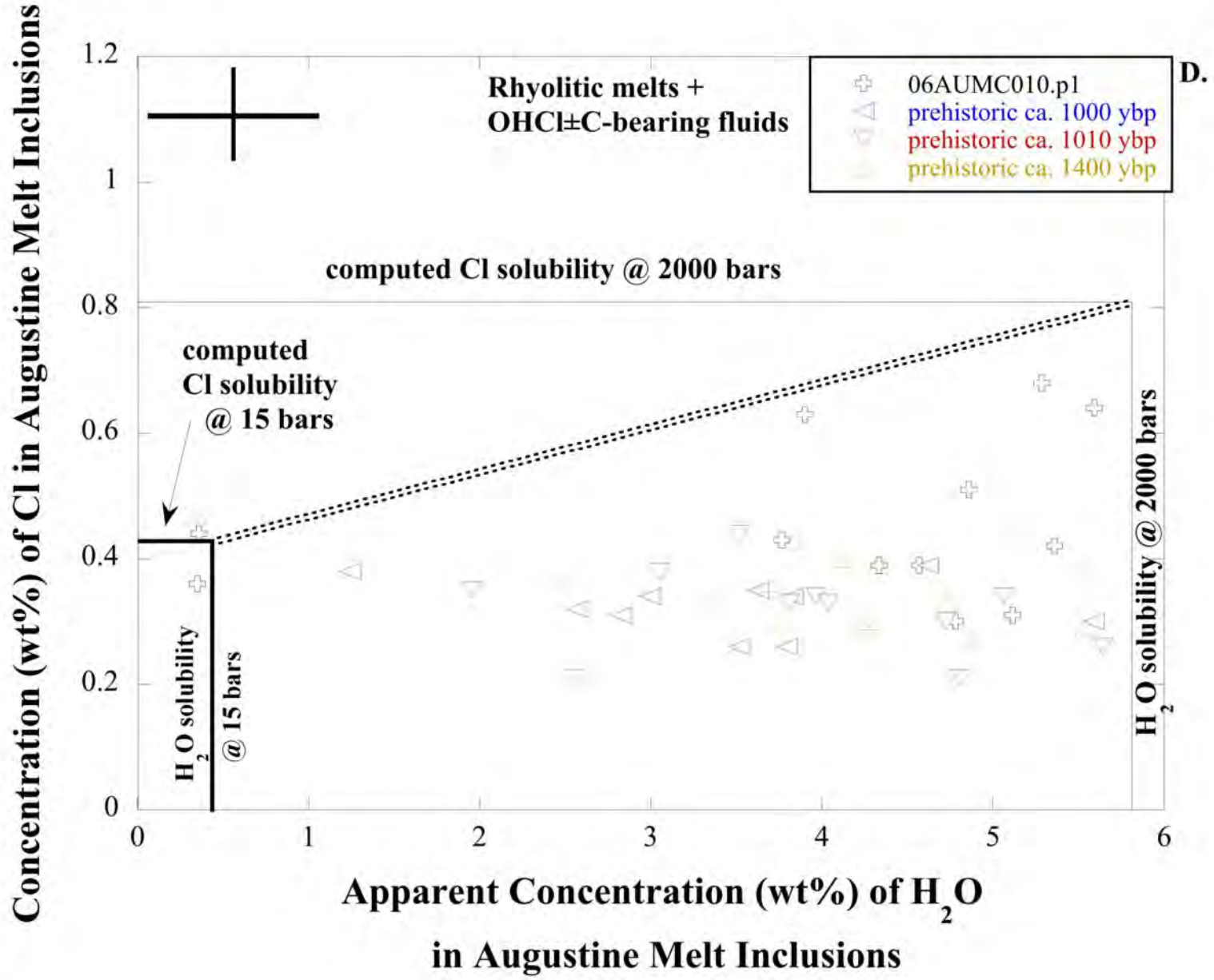
D.
Rhyolitic melts +
OHCl±C-bearing fluids
06AUMC010.p1
prehistoric ca. 1000 ybp
prehistoric ca. 1010 ybp
prehistoric ca. 1400 ybp
computed Cl solubility @ 2000 bars
computed
Cl solubility
@ 15 bars
H2O solubility
@ 15 bars
H2O solubility @ 2000 bars
Concentration (wt%) of Cl in Augustine Melt Inclusions
Apparent Concentration (wt%) of H2O
in Augustine Melt Inclusions
0
0.2
0.4
0.6
0.8
1
1.2
0
1
2
3
4
5
6

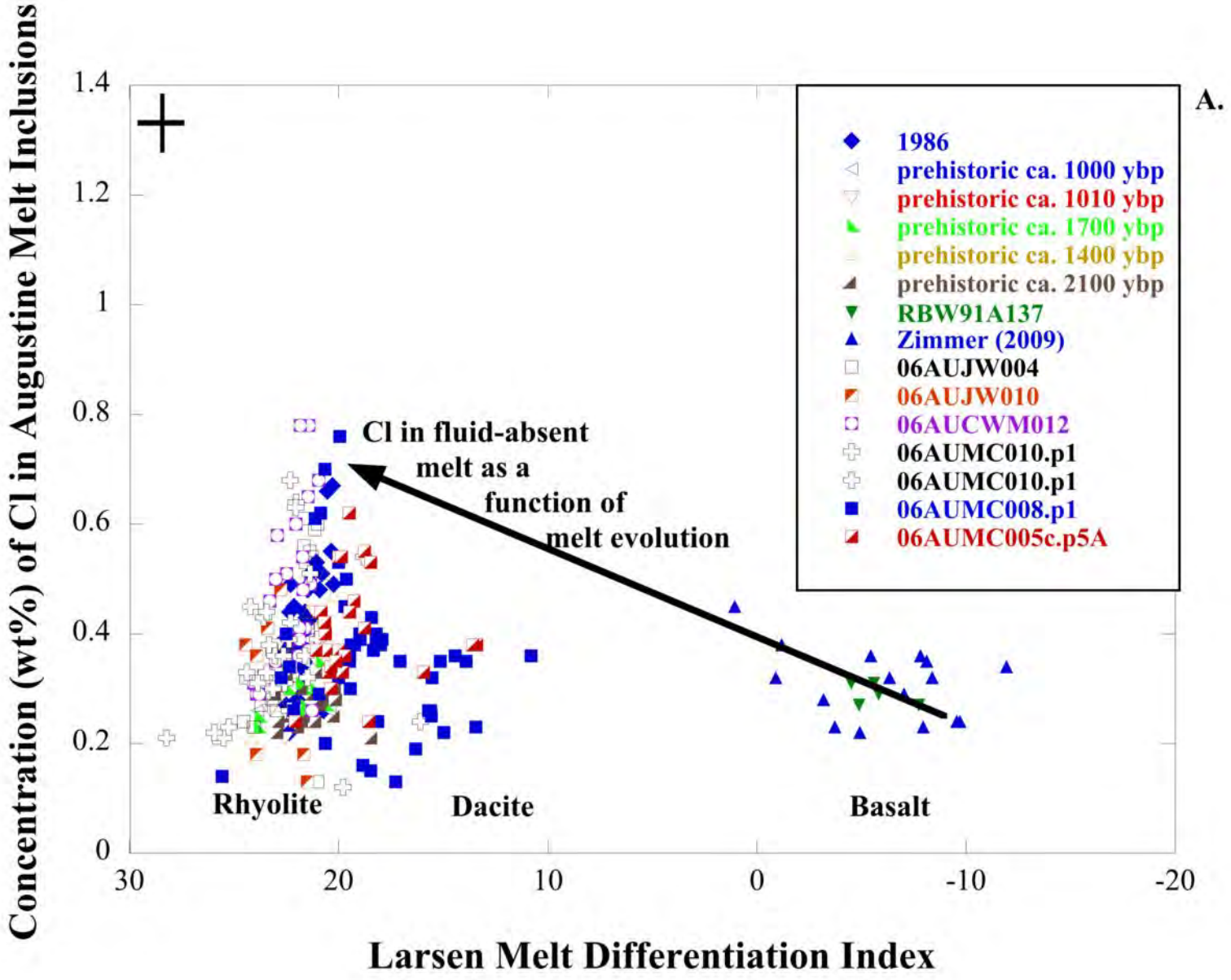
A.
Concentration (wt%) of Cl in Augustine Melt Inclusions
Larsen Melt Differentiation Index
1.4
1.2
1
0.8
0.6
0.4
0.2
0
30
20
10
0
-10
-20
Cl in fluid-absent
melt as a
function of
melt evolution
Rhyolite
Dacite
Basalt
1986
prehistoric ca. 1000 ybp
prehistoric ca. 1010 ybp
prehistoric ca. 1700 ybp
prehistoric ca. 1400 ybp
prehistoric ca. 2100 ybp
RBW91A137
Zimmer (2009)
06AUJW004
06AUJW010
06AUCWM012
06AUMC010.p1
06AUMC010.p1
06AUMC008.p1
06AUMC005c.p5A

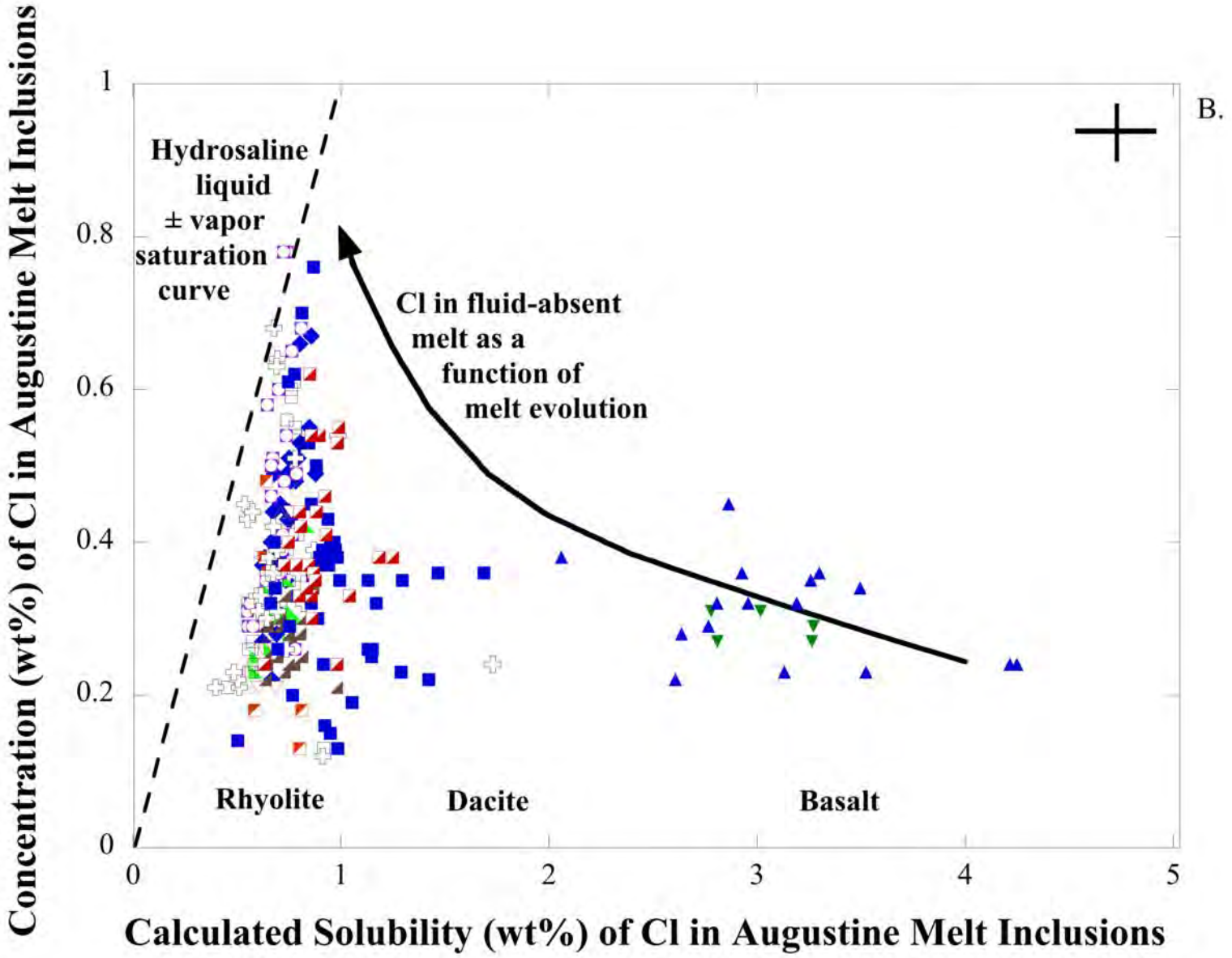
B.
Hydrosaline liquid ± vapor saturation curve
Cl in fluid-absent melt as a function of melt evolution
Rhyolite
Dacite
Basalt
Concentration (wt%) of Cl in Augustine Melt Inclusions
Calculated Solubility (wt%) of Cl in Augustine Melt Inclusions
0
0.2
0.4
0.6
0.8
1
0
1
2
3
4
5

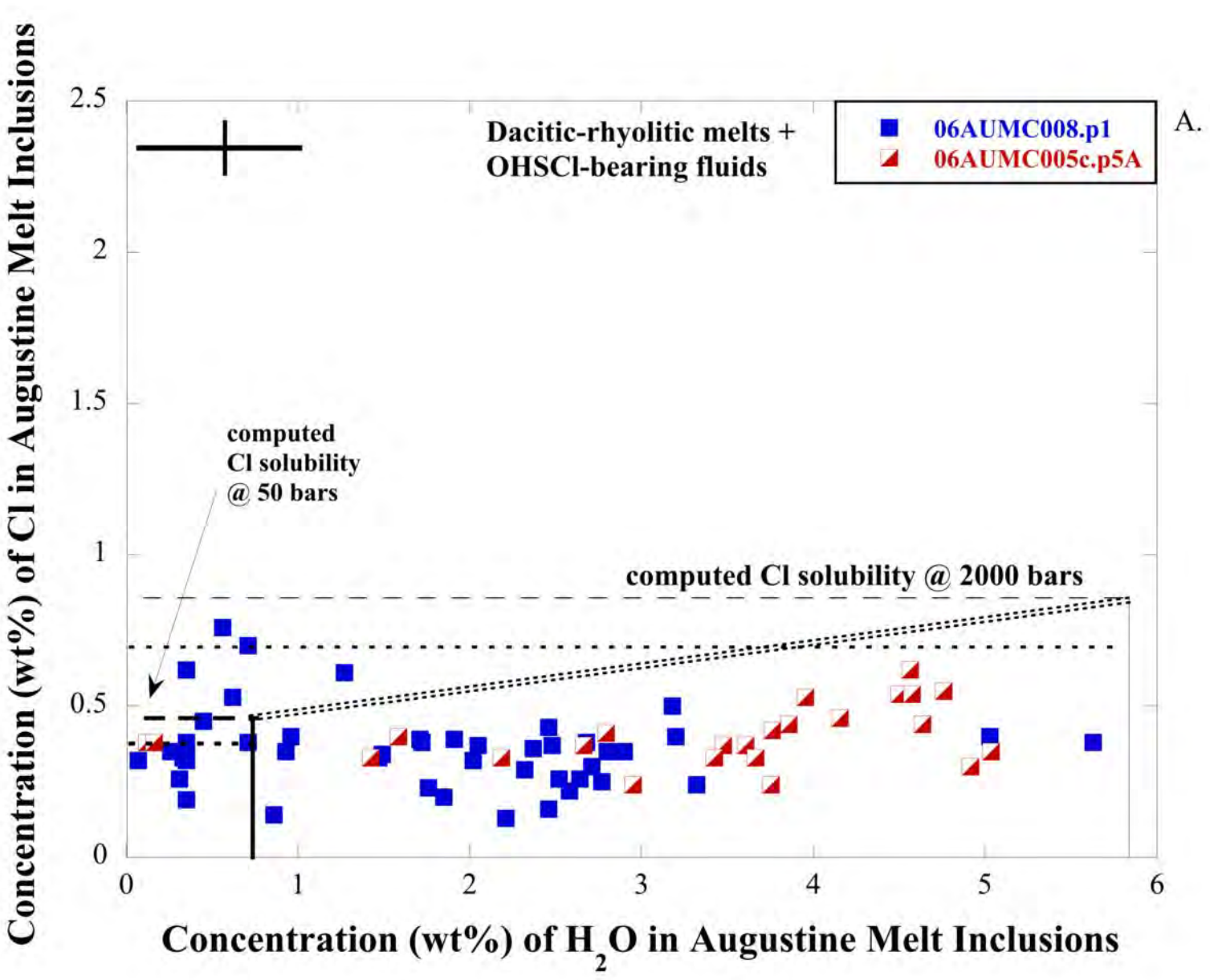
Concentration (wt%) of Cl in Augustine Melt Inclusions
2.5
2
1.5
1
0.5
0
Dacitic-rhyolitic melts +
OHSCl-bearing fluids
06AUMC008.p1
06AUMC005c.p5A
computed
Cl solubility
@ 50 bars
computed Cl solubility @ 2000 bars
0
1
2
3
4
5
6
Concentration (wt%) of H2O in Augustine Melt Inclusions

A.

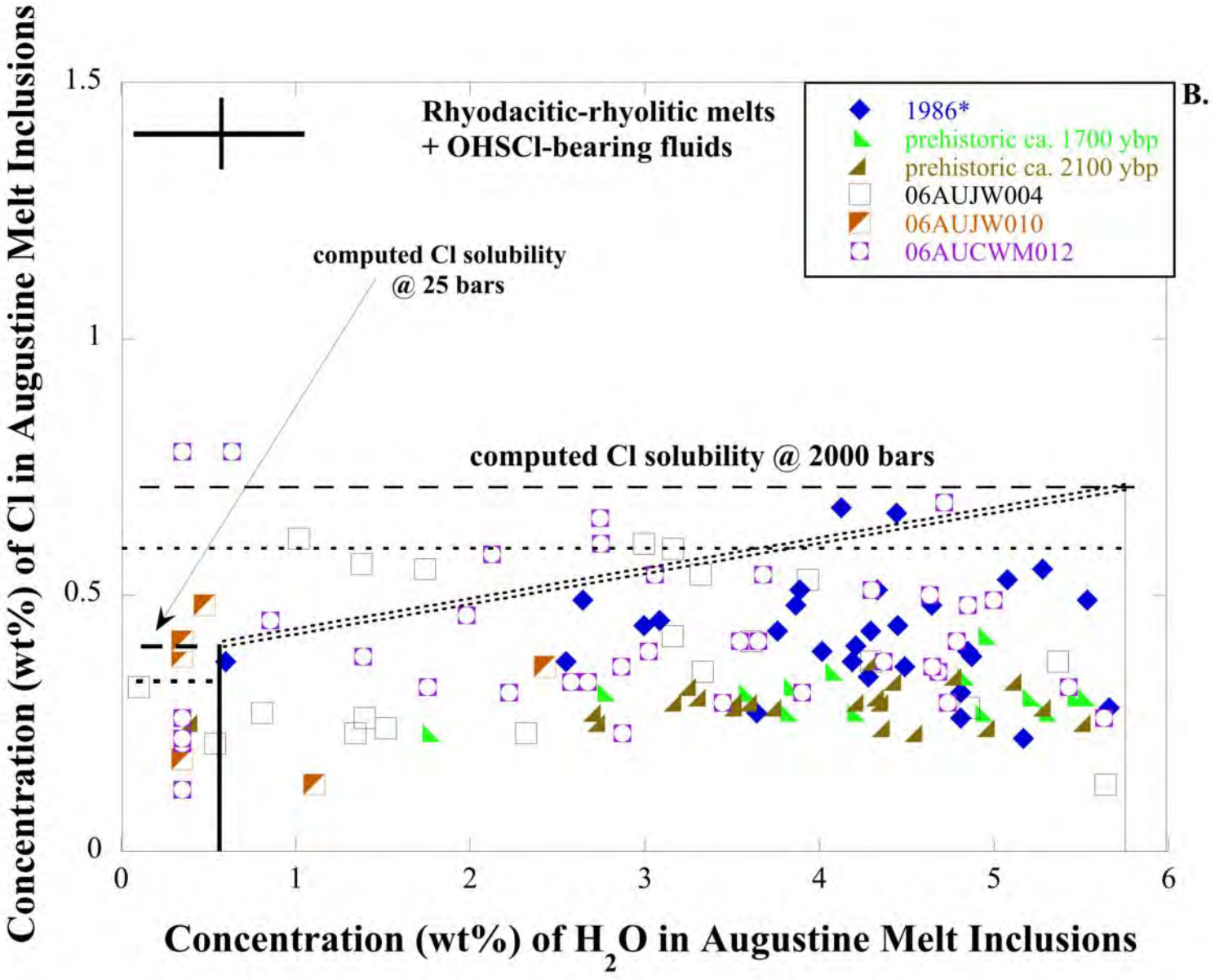
B.
Rhyodacitic-rhyolitic melts
+ OHSCl-bearing fluids
1986*
prehistoric ca. 1700 ybp
prehistoric ca. 2100 ybp
06AUJW004
06AUJW010
06AUCWM012
computed Cl solubility
@ 25 bars
computed Cl solubility @ 2000 bars
Concentration (wt%) of Cl in Augustine Melt Inclusions
Concentration (wt%) of H2O in Augustine Melt Inclusions
0
0.5
1
1.5
0
1
2
3
4
5
6

C.

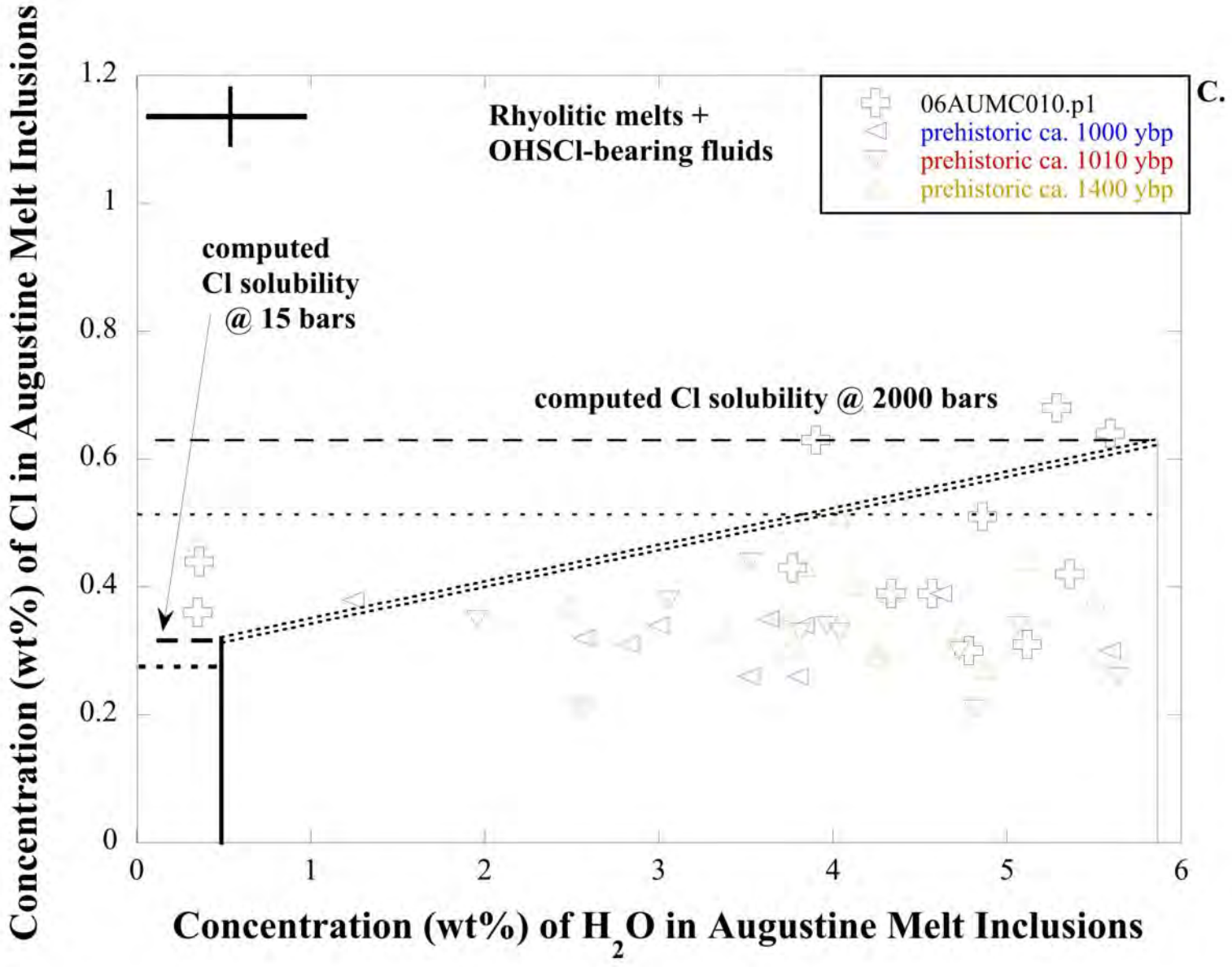
Rhyolitic melts +
OHSCl-bearing fluids
06AUMC010.p1
prehistoric ca. 1000 ybp
prehistoric ca. 1010 ybp
prehistoric ca. 1400 ybp
computed
Cl solubility
@ 15 bars
computed Cl solubility @ 2000 bars
Concentration (wt%) of Cl in Augustine Melt Inclusions
Concentration (wt%) of H2O in Augustine Melt Inclusions
0
0.2
0.4
0.6
0.8
1
1.2
0
1
2
3
4
5
6